Atmospheric Environment 260 (2021) 118482

Contents lists available at ScienceDirect

Atmospheric Environment

journal homepage: www.elsevier.com/locate/atmosenv

Mineral dust and fossil fuel combustion dominate sources of aerosol sulfate in urban Peru identified by sulfur stable isotopes and water-soluble ions

Elizabeth Olson [a,*], Greg Michalski [a,b], Lisa Welp [a], Adriana E. Larrea Valdivia [c], Juan Reyes Larico [c], Jimena Salcedo Peña [c], Huan Fang [a], Kento Magara Gomez [d], Jianghanyang Li [a]

[a] Purdue University, Department of Earth, Atmospheric, and Planetary Sciences, West Lafayette, IN, 47907, USA
[b] Purdue University, Department of Chemistry, West Lafayette, IN, 47907, USA
[c] Universidad Nacional de San Agustin de Arequipa, Department of Chemistry Arequipa, Peru
[d] Universidad Pontificia Bolivariana, Department of Environmental Engineering, Bucaramanga, Colombia

HIGHLIGHTS

- High sulfate aerosol concentration in southern Peruvian city where sulfate is 20% of $PM_{2.5}$ aerosol mass.
- Water-soluble ions and $\delta^{34}S$ isotopes show high natural background levels of sulfate from desert mineral dust (13–26%).
- A Bayesian $\delta^{34}S$ isotope mixing model determined on average 50% of sulfate sourced from oil and coal combustion.

ARTICLE INFO

Keywords:
Sulfur isotopes
South America
Desert aerosols
Developing countries
Source apportionment
High altitude

ABSTRACT

High sulfur emissions in the Central Andes have in the past been attributed to active volcanoes and numerous copper smelting facilities in the region. This study evaluates the contribution of these sources on Arequipa, Peru through an evaluation of aerosol sulfate $\delta^{34}S$ values and water-soluble ions (WSI). The anthropogenic and natural sources of particulate pollution were determined by aerosol filter sampling from four different locations (urban, suburban, industrial, and rural) providing a view of the spatial variability of aerosols within the city. Sulfate (avg. 2.97 $\mu m/m^3$) is the most abundant ion species in the aerosols sampled contributing on average 20% of the molar mass. Ion composition profiles between sampling sites are very similar indicating common sources and high contributions of mobilized local surface salt to the aerosols in this desert region. The regional atmospheric chemistry model (RACM) 0-D run for the area confirms that emissions from fuel combustion sources alone cannot account for the high concentrations of sulfate observed. A combination of the RACM results, WSI data, and a Bayesian $\delta^{34}S$ isotope mixing model determined that the majority of aerosol sulfates in the area are from mineral dust adding to fossil fuel combustion sources. Mineral dust entrainment in the region is likely elevated by the close proximity of open-pit mining and unpaved roads near the city. Marine organic aerosols and smelting located along the Pacific contribute little to Arequipa's aerosol sulfate concentration. While the influence of volcanic sulfate (9% on average) is low, overall natural sulfate (dust, volcanic, and DMS) accounts for 43% of the aerosol sulfate. Therefore, even though the local environment creates high sulfate background levels, a reduction of sulfate aerosol pollution would be possible if fossil fuel emissions were reduced.

1. Introduction

Sulfur emissions to the atmosphere in the form of sulfur dioxide (SO_2) and sulfate (SO_4^{2-}) are of growing concern. In many urban areas SO_4^{2-} from anthropogenic source makes up a significant fraction of $PM_{2.5}$ (Drewnick et al., 2003; Snider et al., 2016). High concentrations of atmospheric sulfate can cause haze events (Chen et al., 2019), acid rain formation (Singer et al., 1993), and be hazardous to human health by increasing rates of mortality and childhood respiratory illness (Hedley et al., 2002; Pope and Dockery, 2012). Understanding the primary emissions and atmospheric chemistry of sulfur species is important for improving air quality in areas with high sulfate pollution levels.

* Corresponding author.
E-mail addresses: elizabethjoy.olson@gmail.com, ejolson@purdue.edu (E. Olson).

https://doi.org/10.1016/j.atmosenv.2021.118482
Received 13 November 2020; Received in revised form 1 April 2021; Accepted 12 May 2021
Available online 25 May 2021

In 2017 the national environmental administration of Peru, Ministerio del Ambiente (MINAM), relaxed the guideline limits of particulate matter and sulfur dioxide, raising concerns about future Peruvian air quality (Hill, 2017; MINAM, 2017). Concerns over this deregulation are compounded by the fact that there have been few studies investigating air quality in Peru (Han et al., 2005; De La Huamán De La Cruz et al., 2019; Pearce et al., 2009; Larrea Valdivia et al., 2019). The city of Arequipa (71°32′05″ W, 16°23′56″ S) located in Southern Peru, has severe air pollution problems that are currently poorly understood. Previous studies using Ozone Monitoring Instrument (OMI) satellite data from the 1990's and early 2000's have attributed the high SO_2 concentrations over southern Peru to regional copper smelters (Carn et al., 2007a; Khokhar et al., 2008). While a 1983 ocean survey off-shore found that non-sea salt sulfate was as high as 23 μg/m^3 in the area, compared to 0.36 μg/m^3 off-shore the rest of the Peruvian and Ecuadorian coasts (Saltzman et al., 1986). SO_2 concentration data from throughout the city of Arequipa, Peru by the local health ministry, reported that the levels between 2010 and 2019 averaged 32 μg/m^3 over 24 h, with hourly averages frequently exceeding 100 μg/m^3 (Arequipa, G.R., 2020). The World Health Organization recommends ambient SO_2 levels should not exceed a 20 μg/m^3 average over a 24-h period (WHO, 2006). Thus, these high levels of local SO_2 impact air quality and pose a risk to human health in southern Peru. While high SO_2 concentrations over southern Peru have been noted, the relative importance of natural (eg. volcanic and DMS) versus anthropogenic (eg. vehicle emissions and copper mining) SO_2 and sulfate sources remains an open question.

SO_2 emissions originate mainly from coal combustion and industrial processes over continental regions are oxidized to secondary sulfate aerosols (Graf et al., 1997; Smith et al., 2001). However, recent studies of aerosol sulfate have found that mineral dust entrained by wind or disturbance of soil surfaces in arid regions (Rodríguez et al., 2011; Zhou et al., 2018) as well as volcanic emissions during active eruptions can be substantial sources of sulfate (Pattantyus et al., 2018; Marshall et al., 2018). These different sulfur sources can have unique sulfur isotope compositions and sulfur isotopes in aerosols has been used in other regions to constrain the relative importance of sulfur emissions sources ((Norman et al., 1999, 2006); Guo et al., 2010; Li et al., 2018, 2020; Rempillo et al., 2011; Xiao et al., 2014). In this study, natural sources of atmospheric sulfate (eg. desert dust and volcanism) and anthropogenic sources (eg. coal and oil) are evaluated and identified for the city of Arequipa using ion abundances, sulfur isotopes, emission inventories, and chemical transport modeling.

2. Methods

2.1. Study area

Arequipa, Peru (Fig. 1) is located 2350 m above sea level (masl) and is the second most populated city in Peru with a population of ~1 million people. The climate is predominantly dry throughout the year (April–December) with annual precipitation averaging ~100 mm that almost exclusively occurs during a rainy season which extends from January to March (Fig. 2).

2.2. Sulfur emissions inventory

The Arequipa region has both anthropogenic and natural SO_2 emissions. Anthropogenic SO_2 emissions are based on a single SO_2 emission inventory conducted in 2005 and are estimated to be 7116 tons/year (DIGESA, 2005). Known SO_2 point sources are dominated by cement production, contributing 42% of total SO_2 emissions (2,968 ton/year), followed by textile production at 5% (368 ton/year), steel lamination and cutting at 2.8% (203 ton/year) and paper production with 2.5% (179 ton/year). Mobile sources contribute 40% of total SO_2 emissions. Diesel fuel is used by 31% of the vehicle fleet in Arequipa and contains less than 50 ppm of sulfur (DIGESA, 2005). The most common gasoline is

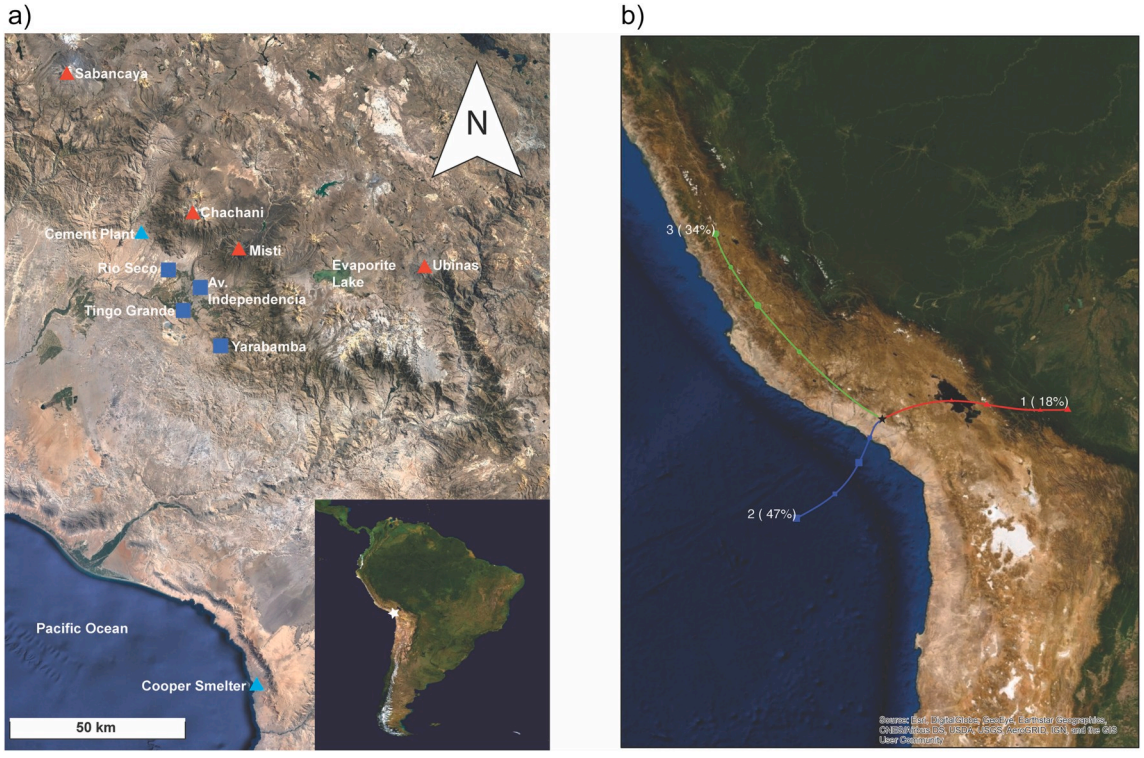

Fig. 1. **(a)** The four air sampling site locations in Arequipa, Peru (blue squres). Potential point sources of primary sulfate are evaporite lakes and desert landscape and possible secondary sulfate sources from oxidation SO_2 including regional volcanic activity (red triangles) and anthropogenic emissions from cement production plant fueled by coal and cooper smelter (blue triangle). (b)The percentage of 48-h air mass origins for 2018 determined using HYSPLIT Lagrangian back trajectory analysis. (For interpretation of the references to colour in this figure legend, the reader is referred to the Web version of this article.)

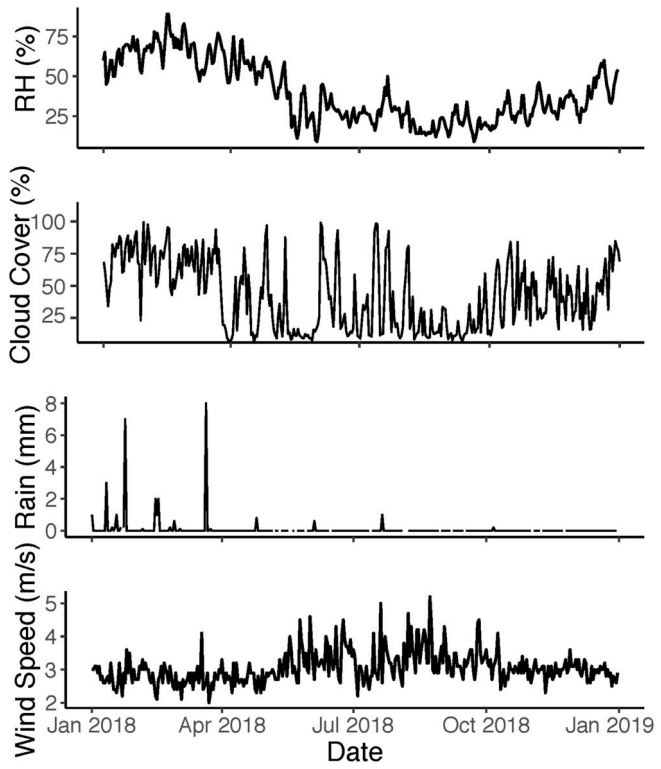

Fig. 2. The 2018 meterological conditions for Arequipa, Peru. Data plotted are daily averages for all parameters except rainfall which is the daily total.

84 octane number, and at the time the inventory was performed sulfur content was around 200 ppm.

The emissions inventory described above excludes important natural regional sulfur sources, either as SO_2 emissions that can produce secondary sulfate or naturally occurring primary sulfate. Primary SO_4^{2-} is preformed sulfate from surface sulfate minerals (i.e. gypsum, anhydrite), evaporate sulfates, sea salt aerosols, and sulfate emitted directly by combustion. A potential large natural source of SO_2 and secondary sulfate is local volcanic emissions. Southern Peru is a center of Andean volcanic activity. Three volcanoes surround the city, Misti (E 20 km), Sabancaya (NE 68 km) and Ubinas (SE 70 km) which emit large amounts of SO_2 (Moussallam et al., 2017). Annual average emissions from 2005 to 2015 based on the Ozone Monitoring Instrument (OMI) NASA's Aura satellite data for Sabancaya are estimated to average 87 tons per day (t/d) ($1\sigma = 158$) and Ubinas averaged 222 t/d ($1\sigma = 252$) (Carn et al., 2017b). The close proximity of these volcanoes to Arequipa make them potentially large sources of local SO_2 and aerosol sulfate. The HYSPLIT dispersion model was run for the 2018 sampling days to determine the potential of ash deposition over the city of Arequipa from the actively erupting Sabancaya volcano (Stein et al., 2015).

Another source of natural sulfate is primary sulfate that can be locally generated by entrainment of desert surface salts (Pueyo et al., 2001) and is a major component of local soils (Li et al., 2019; Rech et al., 2003; Wang et al., 2014). Dust generated by surface disturbance including vehicle traffic on unpaved roads, construction, high winds, and mining is therefore a potential source of aerosol sulfate in the region. To access wind entrainment, back trajectory analysis was done using the NOAA hybrid single-particle Lagrangian integrated trajectory (HYSPLIT) model (Stein et al., 2015). Trajectories were run for 48 h at 200 m arrival height for each day of 2018. All trajectories were then combined via HYSPLIT cluster analysis to determine the principal wind directions over the sampling period (Fig. 1).

2.3. Gas-phase photochemistry

In order to leverage the SO_2 emissions inventory data to understand aerosol sulfate precursors, it is necessary to simulate the photochemical conversion of SO_2 to SO_4^{2-} this was modeled using the Regional Atmospheric Chemical Model, a 0-D box model (Stockwell et al., 1997). This model contains gas-phase chemical reactions using rate constants from laboratory measurements and outputs the seasonal differences in photochemical production of aerosol sulfate. The model was run using the 2010–2011 available gas observation data for the city of Arequipa (Arequipa, G.R., 2020). Model input for local meteoric conditions (pressure, relative humidity, etc.) data comes from the Arequipa airport during the same year as our sample collection 2018 (Weather Online Data Center, https://www.woeurope.eu/)(Weatheronline.uk, 2019). This model does not include isotopic discrimination, aqueous phase or heterogenous reactions. While these SO_2–SO_4^{2-} pathways occur in clouds and are important globally (Alexander et al., 2009), in our inland desert study area, in-cloud and sea-salt processes are likely not large contributors. Therefore, we consider the gas-phase only reactions in the RACM to be sufficient to test for the potential change in oxidation rate and therein changes in isotopic discrimination throughout the study year.

Secondary aerosol SO_4^{2-} is formed from SO_2 photo-oxidation in the boundary layer. The RACM model provides important estimates on the fraction of SO_2 oxidation by OH. The sulfur isotopes are a function of the $\delta^{34}S$ value of the source SO_2 and the isotope effects occurring during its transformation to SO_4^{2-}. The oxidation reaction pathway determines the degree of isotopic discrimination, quantified by α ($\alpha = k_{34}/k_{32}$ the ratio of isotopologue rate constants for ^{34}S and ^{32}S), between the source SO_2 and sulfate product (Gankanda et al., 2016; Harris et al., 2013). Oxidation of SO_2 to sulfate by gas-phase OH radicals has an $\alpha = 1.0081$ while for the various aqueous oxidation reactions it ranges $\alpha = 0.9894$ to 1.0151 (Harris et al., 2012) resulting in differing degrees of isotopic discrimination.

The effective sulfur isotope discrimination between the reactant SO_2 and the product SO_4^{2-} depends on the fraction of SO_2 that is oxidized and can be estimated using a Rayleigh distillation model (Rayleigh, 1896; Mariotti et al., 1981)

$$\delta^{34}S_{SO4} = \delta^{34}S_{SO2} - \varepsilon_{SO4/SO2} \times \ln(f) \times f/(1-f) \quad (1)$$

here $\delta^{34}S_{SO4}$ and $\delta^{34}S_{SO2}$ are the $\delta^{34}S$ values of the aerosol SO_4^{2-} and SO_2 source gas, respectively, $\varepsilon_{SO4/SO2}$ is the isotope discrimination factor for the SO_2 to SO_4^{2-} conversion (ε ‰ $= 1000(\alpha\text{-}1)$), and f is the fraction of SO_2 that is unreacted, which for Arequipa ranges from 0.03 to 0.10 (based on the RACM model results shown in section 3.2). The $\ln(f) \times [f/(1\text{-}f)]$ term has an average value of −0.97 and a range of ± 0.03 so Eq. (1) can be reduced to

$$\delta^{34}S_{SO4} = \delta^{34}S_{SO2} + \varepsilon_{SO4/SO2} \quad (2)$$

The value of $\varepsilon_{SO4/SO2}$ for the SO_2 + OH reaction ranges from +8.9 to +10.6‰, (Tanaka et al., 1994; Harris et al., 2012, 2013). Therefore, based on RACM results that the fraction of SO_4^{2-} by aqueous phase oxidation itself is small (section 3.2) and we assume an $\varepsilon_{SO4/SO2}$ = +10‰, the average of these experimental values.

2.4. Aerosol sampling

Aerosol filter samples were collected periodically throughout 2018 at four sites throughout the city (Fig. 1). Avenida Independencia (AI) is located in the city center where traffic congestion is very heavy during the week. Rio Seco (RS) is in the industrial district where borate pesticide manufacturing plants, quarries, brick kilns, tanneries, and chicken processing plants are located. This district is also located near the main highway by which trucks and buses exit the city. It is also important to note that many of the roads in this district are unpaved. Tingo Grande (TG) is a suburban development located in the western edge of the city

on the slopes of Cerro Verde (2600 masl) and is 6 km north of a large open pit copper mining operation. Yarabamba (YB) is a small town located 15 km outside of the city center surrounded by rural farmland and is 9 km east of the open pit copper mining operation. Samples were collected using a single high-volume air sampler (ECOTECH ECO-HVS3000) fitted with a standard 2.5 μm size selective inlet, moving between sites operating on rooftops (~8 m from the surface). Daily sampling was conducted for three consecutive days at one location (~24 h each) before moving the sampler to the next site in the rotation. Sampling from January to November an average of twenty daily samples was collected at each site. Sample volume averaged 1102 m^3 and flow rate was monitored throughout sampling by the sampler data logger. Low flow rate occurred on two occasions due to power shortages and those filters were discarded. The filter media was either pre-combusted quartz fiber filters (20.3 × 25.4 cm, Whatman, USA) or Teflon filters (PALL, Switzerland).

2.5. Sampling natural potential S sources

Surface sulfates were collected along a transect from the coast to the city from 10 cm below the surface in order to avoid modern pollution source contribution as described in Rech et al. (2003). A 3 g sample of surface sediment was dissolved in 50 ml of deionized water and sonicated for 1-h. Samples were then filtered (0.45 μm) prior to analysis. A sample of brine water was taken from the mined high-altitude evaporite lake above the city for comparative analysis. Waters of dissolved surface salts and the lake water were analyzed using the same methodology as aerosol filter samples detailed below.

2.6. Ion and sulfur isotope analysis

All samples (filter and surface soil extracts) were analyzed for water soluble ions using established techniques. One-tenth of each 8 x 10 in aerosol filter was cut and soaked in 15 mL of Milli-Q water for 20 min, to dissolve all the water-soluble materials. The solution was filtered to remove particles 0.45 μm or larger. A 3 mL aliquot of the filtrate was diluted with 7 mL of Milli-Q water and analyzed for anion and cation concentrations via ion chromatography (Metrohm 940 Vario Professional). Anion eluent was a sodium carbonate buffer (3.2 mM Na_2CO_3 and 1.0 mM $NaHCO_3$) and cation eluent was an oxalic acid solution (3.5 mM). The accuracy and precision of the analysis was less than 0.3% and 0.3 ppm, respectively, based on replicate analysis of standard solutions.

A split of each of the extract solutions was used to precipitate $BaSO_4$ for isotopic analysis. Each sample was acidified with HCl (pH < 2) to remove carbonate, 0.5 ml of a 250 mM $BaCl_2$ solution was added, and the mixture was equilibrated for over 24 h at room temperature to precipitate $BaSO_4$ (Carmody et al., 1998). Measurements of sulfur isotopes ($\delta^{34}S$) were performed via on-line combustion of barium sulfate precipitates (Grassineau et al., 2001) with vanadium pentoxide at 980 °C in an elemental analyzer (Costech EA) coupled to a Delta V Plus Isotope Ratio Mass Spectrometer (IRMS) at the Purdue University Stable Isotope facility. Data were normalized to the Vienna Canyon Diablo Troilite (VCDT) scale using two international reference standards (IAEA-SO5 = 0.5‰ and IAEA-SO6 = −34.1‰). Precision was assessed using an internal laboratory standard of $BaSO_4$ and was better than 0.4‰ for all analyses (n = 44).

2.7. Bayesian source apportionment model

A Bayesian stable isotope source apportionment mixing model was used to determine possible combinations of aerosol sulfate sources based on end-member source $\delta^{34}S$ values. This was done using the R package Stable Isotope Mixing Models (simmr). This Bayesian model uses a Gibbs sampling Markov chain Monte-Carlo algorithm to incorporate prior probabilities and variability in end-member isotope values (Parnell et al., 2013). Since the number of tracers is less than the number of sources, prior source distribution estimates were used to improve model results. Sample *a priori* source distributions were determined before running the mixing model by calculating the contribution of sea salt (as a proxy for DMS) and mineral dust salt aerosol content using equations (3) and (4).

$$Cl^-_{nss} = Cl^-_{meas} - Na^+_{meas} (Cl^-/Na^+)_{seawater} \quad (3)$$

$$SO_4^{2-}{}_{nm} = SO_4^{2-}{}_{meas} - Ca^+_{meas} (SO_4^{2-}/Ca^{2+})_{mineral\ dust} \quad (4)$$

The mass ratio of Cl^- to Na^+ for seawater values are from Chester and Riley (1971) and SO_4^{2-} to Ca^{2+} in local soil values are from this study in Table 1. The difference between Cl^-_{meas} and Cl^-_{nss} (non-sea salt chloride) is the submicron chloride fraction and the value used for the DMS prior. The non-mineral dust sulfate ($SO_4^{2-}{}_{nm}$) and measured sulfate ($SO_4^{2-}{}_{meas}$) difference is then the mineral dust portion.

For volcanic fraction priors, daily SO_2 emissions from the Sabancaya volcano were estimated assuming 5% of SO_2 is oxidized to sulfate and 90% deposition loss along the transport pathway from the volcano to the city based on previous reports and analysis (Rankin, 2012; INGEMMET, 2018). The remaining fraction of observed sulfate was then split between additional priors for coal and gasoline/diesel contribution and, calculated based on the local emissions inventory from 2005 which reported 28.5% of total inventoried SO_2 emissions came from gasoline/diesel and 71.5% from coal (DIGESA, 2005).

The emission source isotopic mixing model can be described by a modified version of the equation set from Han et al. (2016):

$$\delta^{34}S_{total} = f_m\,\delta^{34}S_m + f_{dms}\,\delta^{34}S_{dms} + f_{gd}\,\delta^{34}Sgd + f_{cc}\,\delta^{34}S_{cc} + f_v\,\delta^{34}S_v \quad (5)$$

$$1 = f_m + f_{dms} + f_{gd} + f_{cc} + f_v \quad (6)$$

Above, *f* values are the fractions of each source to the total and the $\delta^{34}S$ is the estimated mean of each source. The subscripts in Eqs. (5) and (6) are *m* mineral dust, *dms* dymethalsulfide, *gd* gasoline/diesel combustion, *cc* coal combustion and *v* volcanic. The Bayesian model then uses the priors and $\delta^{34}S$ values to estimate posterior source contributions for each sample in our study accounting for the variance of each end-member isotopic value. End-member $\delta^{34}S$ values were selected based on measurements of local sulfate and information available in the literature. End-member $\delta^{34}S$ values and ranges are mineral dust (+7.4 ± 3‰), dms (+19.5 ± 2.5‰) (Amrani et al., 2013; Calhoun and Bates, 1989; Calhoun et al., 1991; Krouse and Grinenko, 1991; Oduro et al., 2012), gasoline/diesel (−3 ± 5‰) (Forrest and Newman, 1973; Forrest and Newman, 1973; Krouse, 1977), coal (+6 ± 3‰) (Krouse and Grinenko, 1991; Hong et al., 1993; Chou, 2012; Han et al., 2016), and volcanic (−1.6 ± 6‰) (Echavarria et al., 2006; Marini et al., 2011; Moussallam et al., 2017). For more information, see Supplemental Materials S1.1.

3. Results and discussion

3.1. Water-soluble ions

Sulfate and nitrate were the main identifiable anions in the aerosol

Table 1
Molar ratios of major ions to sodium in sea water, aerosols, and local mineral dust.

	Cl^-/Na^+	K^+/Na^+	Mg^{2+}/Na^+	Ca/Na^+	SO_4^{2-}/Na^+	NO_3^-/Na^+
Sea Water[a]	1.17	0.02	0.11	0.02	0.06	
Arequipa Aerosols	0.33 (±0.20)	0.32 (±0.10)	0.13 (±0.07)	0.60 (±0.24)	0.78 (±0.32)	0.36 (±0.12)
Arequipa Mineral dust	0.71 (±0.23)	0.16 (±0.23)	0.04 (±0.05)	0.13 (±0.15)	0.45 (±0.44)	0.31 (±0.29)

[a] Values from Chester and Riley, 1971

extracts. Sulfate was the dominant water-soluble ion accounting for an average of 20% (range 13–26%) of the molar mass (Fig. 3). After sulfate, the seven other ionic species measured in order of abundance are $Na^+ > NO_3^- > Ca^{2+} > NH_4^+ > Cl^- > K^+ > Mg^{2+}$. The mole fraction of these species varied slightly between sampling sites (Fig. 3). The high percentage of sulfate is consistent with other studies in both continental and coastal areas where sulfate was found to be the main ion when major sulfur sources, such as electrical generation by coal combustion are present (Christoforou et al., 2011; Deshmukh et al., 2011; Hsu et al., 2007; Vasconcellos et al., 2011). In the absence of major sulfur emissions such as coal burning power plants and/or coastal sea spray, anions in aerosols collected in many urban centers are mainly composed of nitrate due to high rates of vehicle NO_x emissions. For example, in the city of Los Angeles (USA) NO_3^-/SO_4^{2-} ratios range from 2 to 5 (Kim et al., 2011) and non-sea salt sulfate NO_3^-/SO_4^{2-} ratios range from 1.7 to 4.8 in many Asian cities (Arimoto et al., 2006). This is not the case in Arequipa where the non-mineral dust sulfate NO_3^-/SO_4^{2-} ratios range from 0.23 to 1.8 with an average of 0.56. Similar ratios have been reported for urban centers such as Shangai, China (Wang et al., 2006), Southern Taiwan (Hsieh et al., 2008), and Durg, India (Deshmukh et al., 2011) where coal burning is common. Thus, there appears to be a significant sulfur source contributing to sulfate aerosol in Arequipa that is atypical relative to other major cities where vehicles are the main N and S emitters.

The majority of ion concentrations correlate with each other and across sites (Table 3) and there is no significant difference between sites (Table S1). Na^+, Ca^{2+}, Mg^{2+}, and K^+ correlate strongly suggesting that they are from a common source. Previous studies have found these cations are primarily attributed to mineral dust/crustal material (eg. Wu et al., 2016). The correlation between these ions combined with low sea salt and high mineral dust fractions indicate that entrained mineral dust is a major source of $PM_{2.5}$ in Arequipa. The major anions NO_3^- and SO_4^{2-} were also correlated, and these anions are usually attributed to anthropogenic pollutant sources. The correlation between these two groups are less strong because in addition to mineral dust these the anions (Cl^-, NO_3^-, SO_4^{2-}) also come from anthropogenic pollutant sources. The notable exception to the overall correspondence between water-soluble ions is NH_4^+ which correlates only with SO_4^{2-} and to a lesser extent Cl^-. The correlation between NH_4^+ and SO_4^{2-} is a common occurrence since gaseous NH_3 can neutralize H_2SO_4 forming ammonium sulfate ($(NH_4)_2SO_4$) and ammonium bisulfate (NH_4HSO_4)(Seinfeld and

Table 3
Correlation coefficients (r) linear regressions between daily ion species concentrations at all sites. Bold values indicate significance $p < 0.005$.

	NH_4^+	Cl^-	K^+	Mg^{2+}	Ca^{2+}	NO_3^-	SO_4^{2-}
Na^+	0.04	**0.69**	**0.48**	**0.67**	**0.67**	**0.77**	**0.70**
NH_4^+		**0.32**	0.10	0.03	−0.04	0.14	**0.57**
Cl^-			**0.29**	**0.28**	**0.50**	**0.57**	**0.57**
K^+				**0.47**	**0.42**	**0.53**	**0.38**
Mg^{2+}					**0.70**	**0.50**	**0.61**
Ca^{2+}						**0.33**	**0.46**
NO_3^-							**0.66**

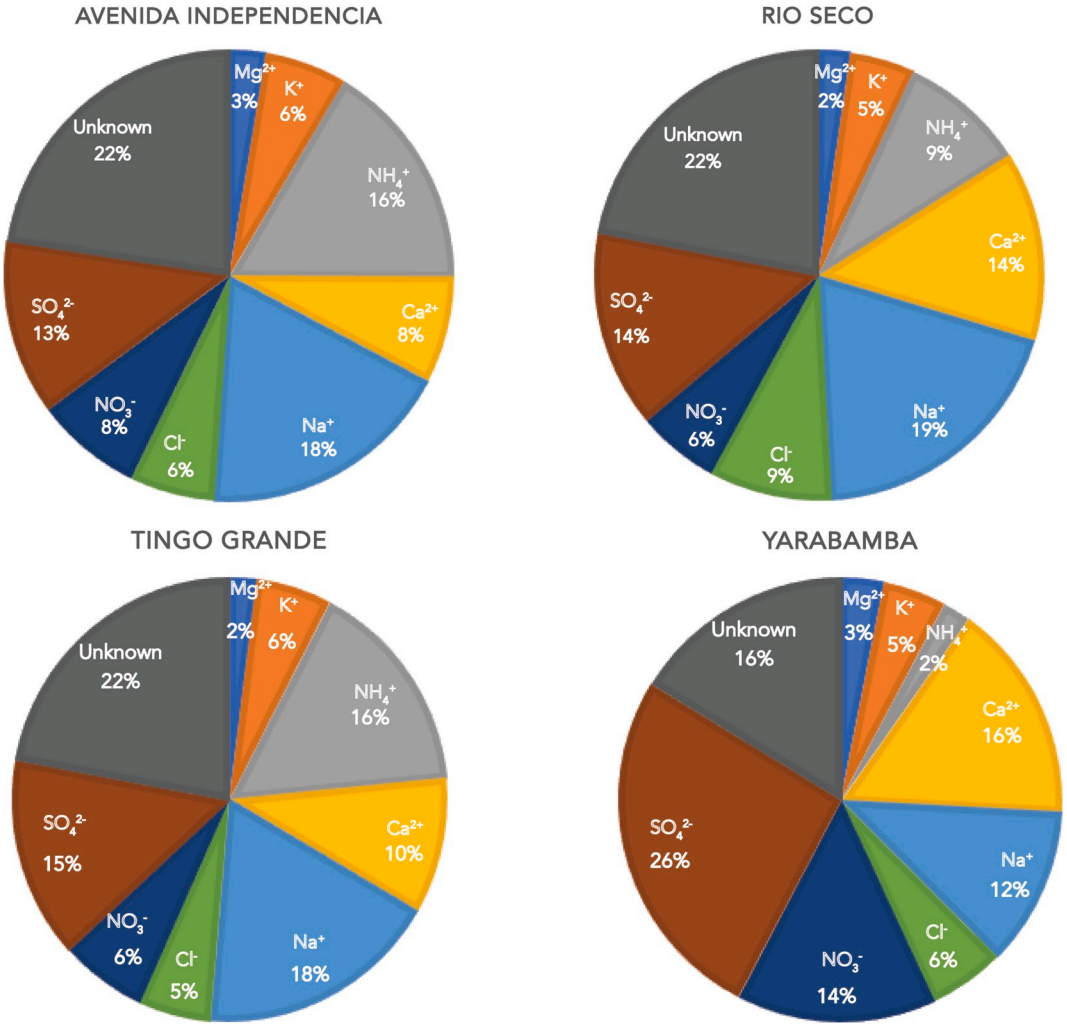

Fig. 3. The average mole fraction of water-soluble ions in $PM_{2.5}$ at each sampling location for 2018.

Pandis, 2016).

An analysis of the ion charge balance shows that there is an anion deficit in nearly all of the samples. The cation:anion ratios were 1.6 and 1.4 for the dry and humid seasons respectively. Potential missing anions include carbonate and organic acids that have proven important for ion balance in other studies (eg. Kerminen et al., 2001). The strongest correlation between the cation excess and cation concentrations was for Ca^{2+} ($r = 0.78$) suggesting the missing anion was associated with calcium. Since ion chromatography cannot detect carbonate (the mobile phase is a carbonate solution) and the presence of a significant amount of organic acids is unlikely given the unvegetated arid environment, the missing anion is likely CO_3^{2-}. The 1.55 cation/anion charge ratio is higher than dust from the southern Atacama Desert (23°S) where it is close to 1 (Li et al., 2019; Wang et al., 2014). The southern Atacama, however, is drier than the Arequipa region and surfaces there are mostly carbonate free except for a few drainages (Berger and Cooke, 1997; Rech et al., 2003). In contrast, Arequipa receives significant moisture (avg. 96 mm/yr) and regional fluvial surfaces are known to contain surficial carbonates in duripans and horizons of carbonate accumulation (Sandor and Furbee, 1996). Surface soils in the desert surrounding the city have been shown to be rich in carbonate minerals (Valdivia-Silva et al., 2009). The mineral dust from local sediment can be entrained by winds, mining, and vehicle use on unpaved roads. Assuming CO_3^{2-} is the missing anion, using the charge balance we estimate that the average CO_3^{2-} concentration in the aerosol samples was 20% on average consistent with entrained dust discussed next.

Two possible sources of non-photochemical aerosol sulfate are sea salt sulfate aerosols and entrainment of terrestrial soil sulfate as dust. In order to quantify the contribution of sea salt and dust sulfate aerosol content the Cl^-/Na+and SO_4^{2-}/Ca^+ ratios were used (Eqs. (3) and (4)). The upper bounds on the sea salt contribution to aerosol sulfate averaged less than 10% for all sites (AI = 9 ± 3%, RS = 8 ± 2%, TG = 7 ± 1%, and YB = 8 ± 5%). Therefore, we assume negligible sea salt contribution to Cl^- since we find very low concentrations of sea salt and the coastal mountain range ~2600 masl likely block marine aerosols before they reach our study area. The blockage of marine aerosols by the coastal range has been observed further south in studies focused on Atacama dust sources (Li et al., 2019; Wang et al., 2014). The terrestrial dust portion of aerosol sulfate estimated from SO_4^{2-}/Ca ratios is 19 ± 9% on average, the lowest average terrestrial input was found at the rural town of YB = 13 ± 9% and the highest input was at the industrial park of RS = 26 ± 13%. The high terrestrial input at the RS site was attributed to unpaved roads in the area, its location upwind of the open desert, and the presence of multiple mineral processing plants in the district. At the urban sites of AI and TG, the terrestrial average is 18.5 ± 8%.

There were no obvious seasonal trends in water-soluble ion concentrations in the $PM_{2.5}$ samples. However, using Eq. (4) to calculate the mineral dust aerosol fraction of SO_4^{2-} we find an increase in terrestrial dust during austral winter. The average mineral dust input for May–October is 29.4% ($\sigma = 21$, $n = 22$) of aerosol sulfate while the rest of the year the average mineral dust input is 14.4% ($\sigma = 9.7$, $n = 48$). This may be due to changes in local wind strength. During austral winter, average windspeeds of 3.2 m/s (May–October) are greater than the other half of the year when the average is 2.8 m/s (Fig. 2). Further, during austral winter, high wind days occur more often with 68% of days above the annual average of 2.9 m/s. Although $PM_{2.5}$ particles are typically dominated by anthropogenic sources, in desert environments, mineral dust is a substantial contribution even in the finer fractions (Gaita et al., 2014; Osornio-Vargas et al., 2011; Shahid et al., 2016; Shaltout et al., 2013; Wu et al., 2012). This increase in mineral dust material does not correspond to a change in $\delta^{34}S$, which is not surprising given the dust average $\delta^{34}S$ (+7.4‰) is very close to the mean aerosol filter $\delta^{34}S$ value (+8.4‰).

The main aerosol cation was Na^+ (avg. 0.85 ± 0.42 μg/m^3) and it is correlated with Cl^- (Table 3) likely from halite (NaCl) surface mineral deposits common in the area (eg. Voigt et al., 2020). Unlike sodium, chloride is not conserved because chloride depletion can occur in areas where pollution is high due to the presence of photochemically produced HNO_3 and H_2SO_4. These strong acids react on NaCl forming $HCl_{(g)}$ and $NaNO_{3(s)}$ and $NaHSO_{4(s)}$ displacing chloride ions from the aerosol phase (Eriksson, 1960; Liu et al., 2005; Quinn and Bates, 2005; Wang et al., 2005). The chloride depletion (Cl_{dep}) by secondary atmospheric processes can be evaluated using the following equation from Quinn et al. (2000):

$$\%Cl_{dep} = ([Cl_{ss}^-] - [Cl_{meas}^-]) / [Cl_{ss}^-] \times 100\% \quad (7)$$

Where $[Cl_{ss}^-] = m \times Na^+_{meas}$, Cl_{ss} is the concentration in local soil mineral dust and m is 0.48, the molar ratio of Cl^-/Na^+ in local mineral dust from soil multiplied by the measured sodium (Na^+_{meas}) molar concentrations in aerosol filter samples. The average Cl_{dep} increases downwind of the urban area, with the upwind RS site having the lowest Cl_{dep} (34 ± 30%), while near the urban center TG (59 ± 27%) and AI (58 ± 14%) values are higher, and the highest depletion occurred at the rural site YB (77 ± 9%). The cause of this pattern in Cl_{dep} is unknown but we can explore several potential factors that may contribute. One explanation is that mineral dust can directly neutralize acidic aerosols and result in measurable differences in aerosol acidity as shown by He et al. (2018). At the RS site, sulfate mineral dust content is higher (see Table 5) and Cl_{dep} is less than the other sites potentially due to this phenomenon of dust neutralization. An additional factor to consider is the influence of regional transport and aging of anthropogenic sources. Arequipa is located in a basin surrounded by mountains with ~3,000 m in topographic relief between the city and adjacent peaks. There is a persistent diel wind direction from the north and thermal inversions due to topographic relief restricts the air volume into which surface aerosols are dispersed (Meixner and Eugster, 1999). Restricted air flow due to valley and slope wind systems may funnel the higher concentrations of HNO_3/H_2SO_4 emission sources from the urban center downwind through the valley to YB creating more acidic conditions and greater chloride depletion. The accumulation of urban aerosols downwind in valley systems has been found in previous studies (ex. Chen et al., 2019; Wallace et al., 2010; Ziemba et al., 2007).

An important caveat to the Cl_{dep} calculations is that this method assumes that all sodium is sourced from NaCl in local mineral dust. This may not be true at the RS site because there is a large salt milling plant in this part of the city where natural evaporite salt deposits of ulexite ($NaCaB_5O_9{\cdot}8H_2O$) and other salts including halite (NaCl) are being processed into pesticides and fertilizers. These salt mineral deposits are mined throughout the region (Boschetti et al., 2007; Kistler and Helvaci, 1994; Schmitt et al., 2002). Therefore, the Cl_{dep} at the RS may be even lower than these calculations suggest. The ratio of Cl^-/Na^+ is higher for RS (average 0.53) than the other sites (average 0.25), perhaps because of additional halite salt.

In summary, the correlation between all ionic species concentrations and their similar composition at all four sites indicates common sources for local aerosols. The surrounding mountains likely play a role in restricting air flow within the city, contributing to similarities between study sites and potentially concentrating pollutants downwind of the valley as evidenced by the higher Cl_{dep} at the YB site. Dust concentrations are higher during austral winter when wind intensity is greater. Coastal mountains block sea spray therefore WSI likely come from salty desert soils near the study sites. Carbonate from local soil dust is likely the second most abundant species, though it was not measured in this study. WSI data show clear source contributions from mineral dust and coal burning to local aerosol sulfate.

3.2. RACM model

The photochemical production of SO_4^{2-} from SO_2 was estimated using the RACM 0-D photochemical box model. The RACM model was initialized using observed SO_2, NO_x, and O_3 data from the local Arequipa

Health Ministry collected from 2010 to 2011 (Arequipa, G.R., 2020) and temperature, relative humidity (RH), and pressure data from 2018. The emission of SO_2, NO_x, and VOCs was based on local emission inventory (DIGESA, 2005). The model was evaluated for its ability to reproduce the observed SO_2/NO_2 ratios and seasonal and diurnal O_3 variations, which is a good indicator of its ability to predict secondary oxidizing radicals which are the main control on SO_4^{2-} production. The model predicted an average daily $[NO_2]/[SO_2]$ of 2.04, slightly higher but within the standard deviation of the ratio observed by the regional health ministry (1.4 ± 0.66). This small difference is likely due to uncertainty in NO_x removal in the region by photolysis, organic trace gases, and mineral dust reactions. Observed O_3 mixing ratios were also well captured by the model predicting an average OH mixing ratio of ~2 x 10^6 molecules cm^{-3} with variation that mirrors seasonal changes in actinic flux and RH. These OH predictions are in good agreement with observed OH number densities in urban environment eg. Dentener and Crutzen (1993); Ren et al. (2006) Kanaya et al. (2007).

The RACM model predicts the $R_{sox} = [SO_4^{2-}]/[SO_x]$, the ratio of the sulfate concentration to total sulfur ($SO_x = [SO_4^{2-}] + [SO_2]$) that agrees with observed R_{sox} values. R_{sox} is an index for the extent of conversion of SO_2 into sulfate in air parcels (Kondo et al., 2007). Measurements of SO_2 were only available for 35 of the 77 sampling days and at one central location in the city, but the measured 24-h R_{sox} averaged 0.05 ± 0.02, which nearly identical to the RACM predicted average of 0.06 ± 0.02. This suggests that the gas phase chemistry is accurately capturing SO_2 oxidation and that only about 5% of SO_2 was oxidized into SO_4^{2-} over a 24-h period, or 0.3% hr^{-1}. In general, a higher R_{sox} is indicative of an "aged" air mass, one in which the SO_x transport time is sufficiently long that a greater proportion of SO_2 has been oxidized into SO_4^{2-} either in the gas or aqueous phase. The low R_{sox} observed in Arequipa implies that the SO_x has not undergone significant oxidation into SO_4^{2-} indicating that local emissions are important or that the regional oxidation rate is low compared to SO_2 sources (local or regional). This is in general agreement with another study examining boundary layer SO_2 oxidation in a high altitude, arid environment, similar to Arequipa. Francis et al. (2016) measured R_{sox} at a mountain site (1680 masl) in the semi-arid region of western India and found R_{sox} values ranging from 0.04 to over 0.3%. The higher values occurring during the winter month were attribute to long-range transport of SO_x. R_{sox} values are higher in many studies (Bari et al., 2003; Kanaya et al., 2007; Kondo et al., 2007; Ren et al., 2006), on the order of 0.2–0.4, but these tend to be in studies with high regional pollution, such as the Tokyo metropolitan area or the east coast of the United States, where regional transport of anthropogenic S is significant. In contrast, Arequipa is somewhat geographically isolated. The cities on Tacna (Peru) and Arica (Chile), combined population of ~500,000, are roughly 250 km to the south while Lima is 800 km to the northeast thus sulfur sources must be somewhat proximal to the city.

The average 24-h sulfate production predicted by RACM of 2.93 ± 0.91 μg/m^3 over the entire year was close to the observed average of 2.87 ± 1.15 μg/m^3. This indicates that gas phase chemistry is producing sulfate via the SO_2 + OH mechanism that can account for most of the observed aerosol sulfate mass. The model estimates higher sulfate production in the southern hemisphere summer (Jan–Feb) compared to winter due to higher OH number densities. This agrees with the higher observed summer average of 4.0 ± 1.3 μg/m^3 and lower winter average of 2.3 ± 1 μg/m^3. This equates to a summer sulfate production rate of 0.04 ppbv h^{-1} and winter of 0.02 ppbv h^{-1}. These results agree with others who have suggested that, under certain conditions, sulfate produced by the SO_2 + OH mechanism can largely explain sulfate production. Studies on boundary layer SO_2 oxidation in other large cities, New York, USA (summer) Tokyo, Japan (summer), and Mexico City, Mexico (spring) found sulfate production rates between 0.021 and 0.069 ppbv h^{-1} (Bari et al., 2003; Kanaya et al., 2007; Kondo et al., 2007; Ren et al., 2006). Similar rates have been found in SO_2 plume oxidation (Bao and Thiemens, 2000; Daum et al., 1993).

Aqueous phase oxidation of SO_2 is considered the main pathway for sulfate production on the global scale, but several lines of evidence suggest this is unlikely the case at our study sites. Global chemical transport models predict that SO_2 oxidation by H_2O_2 and O_3 in clouds accounts for 64–83% of global sulfate production leaving between 17 and 36% to occur by gas phase OH oxidation (Chin and Jacob, 1996; Chin et al., 2000). Though recent research has suggested TMI catalysis of SO_2 oxidation by O_2 may be a major aqueous phase oxidation pathway (Harris et al., 2013), the H_2O_2 aqueous fraction is still thought to be the major pathway occurring in clouds (Alexander et al., 2002). By contrast regional models that include aqueous phase oxidation of SO_2 in clouds tend to over-predict sulfate production and have brought into question the accuracy of existing aqueous oxidation schemes (Koike et al., 2003; McKeen et al., 2007). Regardless, the aqueous oxidation rate depends on local conditions. For example, off the coast of northern Chile and southern Peru, as much as 98% of SO_2 oxidation was attributed to the aqueous phase and the region average was estimated to be 90% (Yao et al., 2002). This rapid SO_2 oxidation rate was attributed to the fast interaction between S emitted from the surface and the low altitude stratocumulus layer that caps the marine boundary layer (MBL). In coastal southern Peru (and northern Chile), this layer is often at or near the ocean surface and studies have suggested that SO_2 is in clouds for on average ~15 min every hour in this area (Feingold et al., 1998). The cloud deck, however, rarely extends above 1,000 m (del Río et al., 2018) and therefore, does not readily penetrate the Peruvian (Chilean) coastal range (~2,000 masl) except where it is incised by river outlets. While aqueous phase oxidation may be the main oxidation pathway in the coastal fogs (Sträter et al., 2010) common off coastal Peru and Chile, this effect is not likely to be important inland where the fog is largely absent. Indeed, large-scale atmospheric subsidence (Klein and Hartman, 1993) and blockage by the coastal range (Cereceda et al., 2002) are two key factors for the aridity in Arequipa.

Analysis of boundary water vapor availability indicates there was insufficient moisture to facilitate aqueous phase SO_2 oxidation over Arequipa (Fig. 2). The trivial amount of atmospheric water in the region has also been shown by recent analysis of precipitable water vapor over Peru using MODIS and ERA-Interim reanalysis data (Ccoica-López et al., 2019). That study showed that Arequipa has only 0–1 cm of perceptible water the entire year, with the higher amounts occurring in Jan–Feb. Circulation dynamics would also suggest that mixing between clouds and surface in the region is not common. Daytime heating of the western slopes of the Andes tends to induce convective updrafts that advect inland air masses towards the ocean (Garreaud and Muñoz, 2004; Rutllant and Garreaud, 2004). This dynamic is evident in regional sulfur budgets that have shown that inland sulfur exists mainly as SO_2 until it reaches the coast where it is nearly equal split between SO_2 and SO_4^{2-} (Huneeus et al., 2006). This suggests that a mechanism where SO_2 is emitted from the Arequipa surface, mixed to the cloud height, oxidized into SO_4^{2-}, and then mixed back to the surface as a major source of aerosol SO_4^{2-} in the city of Arequipa is highly unlikely.

Boundary layer relative humidity (RH) in Arequipa is also relatively low throughout the year, further limiting possible aqueous reactions on deliquesced aerosols. Aerosols can spontaneously absorb water (deliquesce) at a RH below 100% forming brine layers that can facilitate aqueous phase oxidation of SO_2 (Andreae et al., 1985; Chameides and Stelson, 1992; Li et al., 2020; Wang et al., 2014). Most pure inorganic salts deliquesce when RH exceeds 70‰ (Brandt et al., 1995; Sandor and Furbee, 1996) and mixed organic-inorganic aerosols, typical of urban environments such as Arequipa, require even higher RH for deliquescence (Cruz and Pandis, 2000). Thus, below a RH of 70%, the lack of liquid surface layers inhibits effective aqueous oxidation on existing aerosols. Actually, some of the early research that examined lifetimes of sulfur in the atmosphere suggested that when RH is below 70% that gas phase oxidation was the main mechanism for converting SO_2 into SO_4^{2-} (Henmi and Reiter, 1978). Daily average RH in Arequipa during summer (Jan.–Mar.) averaged 66 ± 6.5% (Fig. 2) but was typically below 40% during the remainder of the year (RH = 36 ± 17%). In fact, there were

only 10 days was there RH above 70%, usually occurring during days when there was precipitation. This would suggest that there were few sampling days where aqueous phase oxidation on deliquesced aerosol in the boundary layer would have been important. There are four sampling days that had the highest sulfate mass concentration that correspond to high relative humidity suggesting that deliquescence and aqueous phase oxidation may have occurred. But these also occur in February when j (O^1D) is highest, as is [H_2O], leading to the highest OH production of year, as evident from the peak in SO_4^{2-} production via SO_2 + OH predicted by RACM (Fig. 4). The RACM model, however, under predicts SO_4^{2-} production on these days so aqueous phase oxidation may play a role in sulfate production on the rare days when RH > 70%. On the other hand, the model also under predicts SO_4^{2-} production in August–September when RH is quite low (<30%) when significant aqueous phase SO_4^{2-} production can be ruled out. Sulfur isotopes suggest that for at least some of these latter samples, the excess aerosol SO_4^{2-} may be derived from soil salts entrained into the atmosphere (see below). The elevated aerosol sulfate mass concentrations observed in Jan–Feb and Aug–Sept. were investigated in terms of regional sources of SO_2 that may have been transported into the Arequipa basin.

Two possible major point sources of SO_2 were identified, the Sabancaya volcano and the copper smelting plant at Ilo to the southwest. Sabancaya is an active volcano located 75 km NNW of Arequipa that constantly emitted SO_2 during 2018 (Fig. 1). Excluding the three anomalous eruptions in February and July, SO_2 monitoring estimated that the volcano emitted an average of about 1800 metric tons of SO_2 per day (INGEMMET, 2020). By comparison the total annual SO_2 emissions by anthropogenic activity in Arequipa is roughly 7,100 tons yr^{-1} or 19.5 tons day^{-1} or 1% of Sabancaya's 2018 daily emission rate. The 2018 Sabancaya SO_2 emissions are roughly 20 times higher than the 87 tons day^{-1} estimated by Carn et al. (2007b) for 2005–2015 based on satellite observations. Sabancaya's activity increased at the end of 2016, new fumaroles developed, and there was a growth in thermal energy (Reath et al., 2019). Ground-based passive differential optical absorption spectroscopy (DOAS) was installed in 2016 as part of the Network for Observation of Volcanic and Atmospheric Change and SO_2 emissions of over 6,000 tons day^{-1} were soon observed (Galle et al., 2010). This SO_2 emission activity continued throughout 2018 and could be a source of high SO_2 and aerosol SO_4^{2-} found in Arequipa if atmospheric transport of these SO_2 plumes was effective. The ability of SO_2 to be transported from Sabancaya to Arequipa was assessed by Rankin (2012) using the HYPLIT dispersion model. Deposition of sulfate from Sabancaya is more likely to reach Arequipa during the summer than the winter because of seasonal shifts in wind direction (Rankin, 2012). Smaller eruptions led to higher ash deposition locally than large eruptions which enter the stratosphere and travel further (Rankin, 2012). We ran HYSPLIT dispersion models for the 2018 sampling days and found there were 37 days in which transport from Sabancaya reached the city of Arequipa. While we found no correlation between sulfate amount during days when transport from Sabancaya was evident, the isotopic value positively correlated to SO_2 emissions when they were greater than 2200 tons/day ($r = 0.76$, $n = 16$, $p < 0.05$).

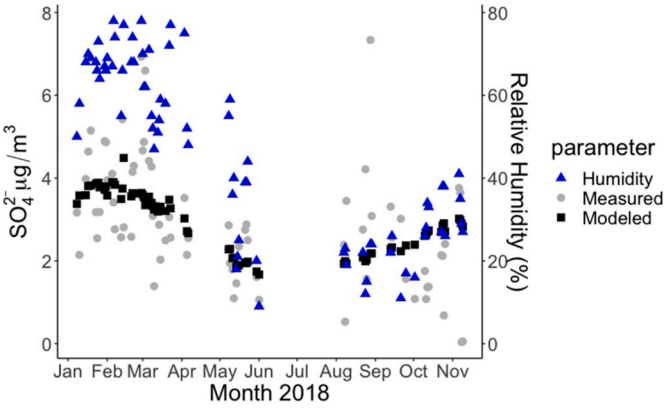

Fig. 4. The observed Arequipa aerosol SO_4^{2-} mass concentration (grey circles) in µg m^{-3} and that predicted by the RACM model (black squares). The average percent relative humidity (RH) measured in Arequipa during the sampling days (blue triangles). (For interpretation of the references to colour in this figure legend, the reader is referred to the Web version of this article.)

Another possible source of regional SO_2 is the large copper smelting operation located in Ilo, Peru 115 km south of Arequipa. Copper smelting releases large quantities of sulfur gases into the atmosphere with ~1.2 tons S per ton of copper produced (US EPA, 1995). Peru is a major producer of copper globally producing 2.4 million tons annually in 2018 and the Ilo copper smelting operation produced 638 kilotons in 2017 (Mining data online, 2020). Large amounts of SO_2 measured off the coast of Ilo were first attributed to this copper facility during the 1980's by Saltzman et al. (1986). Later studies using OMI satellite data from the 1990's and early 2000's showed enhanced cloud cover and high SO_2 emissions ~0.3 Tg yr^{-1} over southern Peru that was also attributed to regional copper smelters (Carn et al., 2007a; Khokhar et al., 2008). SO_2 removal technology was installed on the Ilo smelters between 2003 and 2007 (Boon et al., 2001), which, has greatly reduced SO_2 emissions in recent years with a 25% reduction from 2004 to 2005 (Carn et al., 2007a; Khokhar et al., 2008). Offshore surveys in 2012 found no elevation in concentrations of nss-SO_4^{2-} within range of the plant (Baker et al., 2016). While onshore winds are dominant at Ilo, HYSPLIT forward air mass trajectory analysis by Baker et al. (2016) show that air masses from the coastal plant rarely reach to 2,000 m above ground level and are therefore blocked by the coastal mountain range that reaches elevations over 2,500 m creating a natural barrier between Arequipa and Ilo. The adoption of sulfur scrubbers at local smelting operations and the fact that smelters are located on the coast separated by the coastal mountain range from the valley where Arequipa is located the Ilo copper smelting plant is not likely a major source of local SO_2 in the city of Arequipa.

The RACM model output matches the observed concentrations of sulfur dioxide and our measured sulfate aerosol samples predicting a 5% oxidation rate via the SO_2 + OH mechanism. These results show that aqueous phase oxidation is likely not important for sulfate production locally which is to be expected given the dry atmospheric conditions. The low R_{sox} indicates that air masses in the city are not mature and thus S emission sources are likely local. In addition to anthropogenic emissions within the city, the erupting Sabancaya volcano likely contributes to local sulfate. The Ilo smelting plant was of concern historically but has now reduced its SO_2 emissions and any emissions are probably blocked by the coastal mountains.

3.3. Sulfur isotopes in aerosol sulfate

The $\delta^{34}S$ values of aerosol sulfate ($\delta^{34}S_{sulf}$) were used to further constrain the local sulfur budget. The mean aerosol $\delta^{34}S_{sulf}$ value was +8.9 ± 5‰ with significant variability throughout the year (Fig. 5). To help determine local natural sources of primary sulfate, the $\delta^{34}S$ values for local surface soil mineral dust sulfate (average + 7.4‰ ± 3.1, n = 11), evaporite lake sulfate, and coastal surface sulfate were also

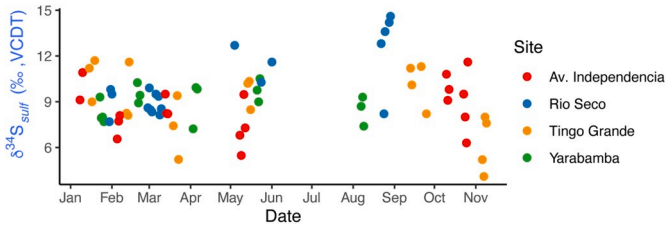

Fig. 5. $\delta^{34}S_{sulf}$ over time at all sites over the 2018 sampling year.

measured (Fig. 6). The isotopic value of coastal sulfate (+16.1‰, n = 1) reflects oceanic salt and DMS sources and is within the range of previous measurements (eg. Bao and Thiemens, 2000). Sulfate (average + 19.7‰ ± 4.5, n = 2) from the Laguna Salinas high altitude evaporite lake surface is similar to marine sulfate values possibly owing to the marine limestones of Jurassic age underlying the salar basin (INGEMMET, 2018; Alván et al., 2018). Similar to our findings a survey of evaporite lakes to the south of our study area used $\delta^{34}S$ and $^{87}Sr/^{86}Sr$ to determine that local salts were derived from rock-water interactions and evaporation of groundwater not marine, volcanic, or atmospheric sources (Rech et al., 2003). Our transect of soil mineral dust sulfate shows that coastal marine deposition does not extend past the coastal mountain range and that inland salts are likely related to weathering of local rock formations.

To assess the relationship between ions and $\delta^{34}S$, correlation coefficients are calculated (Table 4). A statistically significant correlation was found between the aerosol $\delta^{34}S$ value and NH_4^+ indicating a unique end-member source of aerosol sulfate that decreases $\delta^{34}S$ while increasing ammonium, possibly from agricultural fertilizers. The $\delta^{34}S$ also correlates significantly with Mg^{2+} which we attribute to the homogeneous isotope signature of soil mineral dust sulfate since Mg^{2+} aerosols are sourced from crustal material (Fig. 4).

The five highest $\delta^{34}S_{sulf}$ values (14.6–12.7‰) were all from the RS site and the three lowest (4.1–5.2‰) were from the TG site, suggesting that there may have been unique, localized SO_4^{2-} sources at those sites during certain periods relative to the other sites and times. The five anomalously high $\delta^{34}S_{sulf}$ values (avg. 14‰) from the RS site were collected over three consecutive days in August. Field observations led us to believe that these sample values could be the result of a borate processing plant located adjacent to the sampling site that processes evaporite lake materials. A sample of the evaporite sulfate $\delta^{34}S$ indicates that input from this source would increase local aerosol sulfate values as observed. Further, evaporite lake mining operations are more active during the peak of the dry season between August and October. These three outlier days fall directly on a mixing line between evaporite lake and surface soil mineral dust sulfate (Fig. 7). These three outlier samples were not included in our average site Bayesian apportionment model as they do not represent typical conditions.

3.4. Sulfur isotope Bayesian model results and discussion

The results the sulfate source apportionment indicate that the dominant source of sulfate pollution is fossil fuel combustion, despite the high concentration of naturally occurring sulfate in the region (Table 5). Combined oil and coal combustion account for more than half (57%) of the local aerosol sulfate. Primary sulfate from mineral dust is the second largest sulfate aerosol source (19%), followed by DMS (14%) and secondary volcanic sulfate (9%) from local SO_2 emissions contributing to background sulfate levels. Sensitivity analysis comparing the model run with and without prior estimates changed fraction estimates on average 10% and improved the standard deviation by 5% (Table S2).

Table 4
$\delta^{34}S_{sulf}$ and water-soluble ion correlation coefficients (r). Bold values $p < 0.001$.

	Na^+	NH_4^+	Cl^-	K^+	Mg^{2+}	Ca^{2+}	NO_3^-	SO_4^{2-}
$\delta^{34}S_{sulf}$	0.21	**−0.30**	0.17	0.07	**0.34**	0.23	0.17	0.01

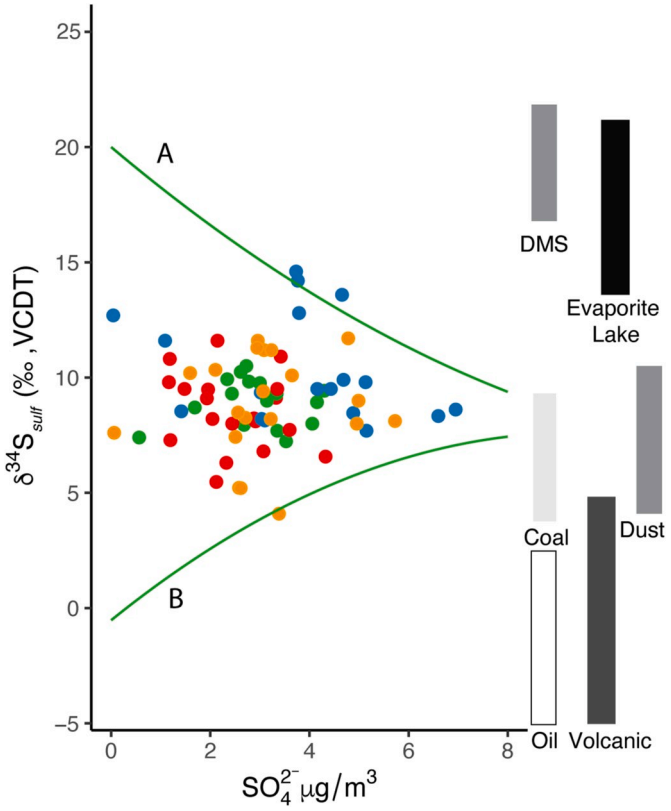

Fig. 7. $\delta^{34}S_{sulf}$ and sulfate concentration in aerosols of Arequipa compared to a ternary mixing model. Curve A is a mixture between sulfate in local evaporite lake deposits, $\delta^{34}S_{sulf}$ = +19.7‰, and local mineral dust, $\delta^{34}S_{sulf}$ = +7.4‰. Curve B is a mixture between volcanic sulfate, $\delta^{34}S_{sulf}$ = −1.6‰, and local mineral dust, $\delta^{34}S_{sulf}$ = +7.4‰.

It is important to note that the range used for end-member values produces uncertainty in the apportionment model. However, this uncertainty is minimized by the iterative Bayesian approach and the standard deviations reported in Table 5 are the ranges for all samples at each site and represent day to day variability as well as the uncertainty inherent in end-member ranges.

The results of the Bayesian apportionment model found that sulfate sources from coal (37 ± 8%) were higher than those from gasoline/

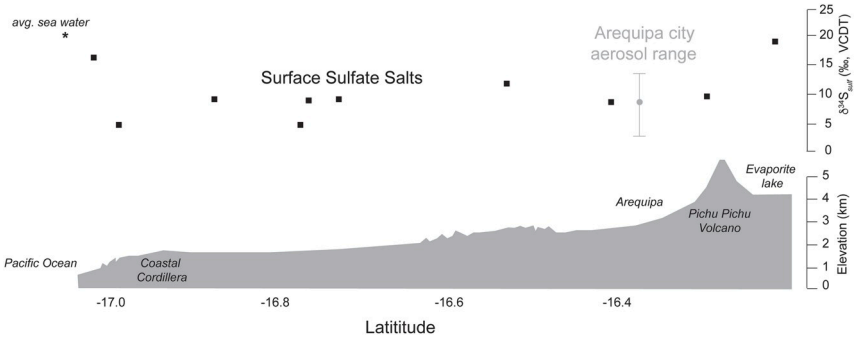

Fig. 6. The $\delta^{34}S_{sulf}$ in sea water (*), surface soil salt mineral dust(■), aerosols from Arequipa city (•), and evaporite lake deposits along a West-East latitudinal transect.

Table 5
$\delta^{34}S_{sulf}$ source apportionment model results from each sample site.

Site	$\delta^{34}S_{sulf}$ (‰)		Soil Mineral Dust SO_4^{2-} (%)		Coal SO_4^{2-} (%)		Oil SO_4^{2-} (%)		Volcanic SO_4^{2-} (%)		DMS SO_4^{2-} (%)	
			f_{prim}		f_{sec}							
	Min	Max	Mean	Sd	Mean	Sd	Mean	Sd	Mean	Sd	Mean	Sd
AI	5.5	11.6	18.0	10.0	42.6	6.6	18.5	5.5	7.4	3.8	13.4	2.2
RS	7.7	14.6	26.0	13.0	42.92	6.7	10.3	3.8	9.6	3.3	10.6	2.2
YB	4.1	11.7	13.0	9.0	23.9	5.4	30.9	5.4	9.6	6.4	21.8	2.6
TG	7.2	10.5	19.0	6.0	40.7	15.5	19.0	9.9	6.5	5.6	14.2	4.6

diesel (20 ± 6%). This result is in agreement with the NO_3^-/SO_4^{2-} ratios of the non-mineral dust aerosol fraction which, fall both above and below the 0.80 ratio indicating that fuel combustion is divided between mobile (eg. Vehicles) and stationary (eg. Coal) sources (Gao et al., 1996; Yao et al., 2002) (Fig. S1). At all sites, the concentration of the non-mineral dust nitrate and sulfate are weakly correlated ($R^2 > 0.25$) suggesting multiple anthropogenic sources of the two species. The molar ratio of NO_3^-/SO_4^{2-} in aerosols is 0.94 on average for all samples but the SO_2 and NO_x emissions data from 2010 in Arequipa found a molar ratio of 1.8 between the gas concentrations (Arequipa, G.R., 2020). The greater abundance of particle SO_4^{2-} can be explained by the addition of primary sulfate from mineral dust (avg. 19%) which is not oxidized from SO_2 gas. The split between mobile and stationary SO_2 emission source is corroborated by all data and models in this study. Further, it agrees with the 2005 emissions inventory which determined that oil burning sources made up 28% of SO_2 emitters and coal 72% (DIGESA, 2005) for anthropogenic sources only, our apportionment results are very similar with oil at 34% and coal 66%.

Mineral dust is the third-largest contributor (average 19%) to atmospheric sulfate. The proportion of mineral dust is highest at the RS site located next to the open desert. Mineral dust is often a substantial fraction in arid desert environments (Gaita et al., 2014; Osornio-Vargas et al., 2011; Shahid et al., 2016; Shaltout et al., 2013; Wu et al., 2012). Paving roads in this part of the city may help to decrease this source. The mineral dust is higher near the urban center sites of AI and TG than the rural YB. A possible explanation for this is that construction in the city contributes to mineral dust entrainment. The high proportion of dust would explain why the RACM secondary sulfate predictions were lower than observed and the correlation between terrestrial elements in our WSI data. Dust entrainment in this arid environment is of greater importance than volcanic or oceanic DMS sulfate.

The volcanic emissions average 9% of the total $PM_{2.5}$ sulfate across all sites. This result is surprising given the high rates of volcanic activity in the study area (Carn et al., 2017a). However, the volcanic peaks sit a minimum of 3,000 m in altitude above the city and this height makes it difficult for emissions to be mixed down to the surface. This phenomenon was also observed at the Popocatepetl volcano near Mexico City (Yao et al., 2002). Further, the proportion of volcanic sulfate is highest at the rural YB site were the contribution from other anthropogenic sources is smaller showing that is more important outside of the urban area. This finding supports previous work by Rech et al. (2003) that found surface sulfate in the Atacama Desert was not derived from volcanic sources. While the volcanic activity in the area is definitely a source of aerosol sulfate locally, historical satellite data indicates local smelting operations emitted large amounts of SO_2. The $\delta^{34}S_{SO2}$ values of smelting SO_2 emissions are indistinguishable from volcanic values. Previous studies have found smelting produces $\delta^{34}S_{sulf}$ values ranging from −3.8 to +3.4‰ (Grey and Jensen, 1972; Mayer et al., 2007). The adoption of sulfur capture technology has led to a reduction of SO_2 emissions (Carn et al., 2007a; Khokhar et al., 2008) at local smelting operations and the fact that smelters are located on the coast separated by the coastal mountain range from the valley where Arequipa is located, we attribute the lower $\delta^{34}S$ contribution to volcanic emissions. While, smelting may no longer be a major local sulfur dioxide emitter, future emissions survey should include these sources that have been excluded in the past (DIGESA, 2005). Future research looking at lead isotopes may be able to distinguish volcanic from smelting aerosol inputs since lead isotope discrimination during smelting processes can identify natural versus processed sources (Félix et al., 2015).

DMS accounts for 15% of aerosol sulfate in our study. While DMS has been shown to travel long distances inland, the coastal mountain range effectively blocks the transport of oceanic sea salt aerosols from the interior valleys. DMS concentrations are elevated off the coast of Southern Peru during the months of January, June and July (Lana et al., 2011). DMS to SO_2 conversion varies as a function of temperature from 100 to 10% efficiency between 28 and 0 °C, respectively (Bandy et al., 1996; de Bruyn et al., 2002), therefore we would expect the greatest contribution of DMS-derived sulfate to occur during austral summer in January when SO_2 conversion is highest. During the summer months however the winds are primarily from the east blowing offshore diminishing atmospheric transport efficiency. Therefore, low DMS contributions are expected since winds do not favor inland transport when coastal production is highest.

In summary, the Bayesian apportionment model shows that 57% of atmospheric sulfate originates from anthropogenic fossil fuel emissions in Arequipa. The remaining 43% comes from natural sources of mineral dust, volcanic, and DMS fluxes. The high abundance of natural sulfate in the atmosphere in Arequipa means that health limits for particulate matter concentration are exceeded much more quickly in this region. As a result, in order to maintain good air quality in the city, emissions regulations for sulfur emissions should be more stringent.

4. Conclusions

This study demonstrations how combining water-soluble ion (WSI) with sulfur isotope data can be used to trace sources of air pollution. The WSI data show that mineral dust that contributes a large portion (~20%) of local atmospheric sulfate. The $\delta^{34}S_{sulf}$ analysis shows that oil and coal combustion together account for just over half local aerosol sulfate. Together mineral dust and fossil fuel combustion account for on average 70% of sulfate aerosols in this region. While previous research reports high volcanic SO_2 emissions we find it is less important (~8%) than urban combustion emissions (~50%). Volcanic emissions likely contribute less due to the high elevation of these sources 3,000 m above the city and low oxidation rates. Agreement between our apportionment and RACM models with previous emissions inventories and gas measurements provides confirmation that this study captures the variable sources of local sulfur emissions in this poorly understood region.

Studies focused on air quality in developing countries such as this one are particularly challenging because there is a paucity of data available. Here we have combined data from multiple sources in order to better understand the cause behind high atmospheric sulfate in southern Peru. Within the city of Arequipa, it appears that anthropogenic emissions exacerbate sulfate concentrations in an area already prone to high natural sulfate due to entrainment of mineral dust sulfate and to a lesser extent, volcanic activity. These findings highlight the fact that emissions standards should be tailored to the specific environments. Future work in southern Peru should focus on quantifying source emissions using gas

concentration measurements taken in tandem with filter samples, improved emissions inventories, and direct source characterization via sampling near emission sources.

CRediT authorship contribution statement

Elizabeth Olson: Conceptualization, Methodology, Writing – review & editing, Formal analysis, Investigation, Visualization, Data curation. **Greg Michalski:** Conceptualization, Methodology, Formal analysis, Writing – review & editing, Visualization, Funding acquisition, Project administration. **Lisa Welp:** Conceptualization, Writing – review & editing, Funding acquisition, Project administration. **Adriana E. Larrea Valdivia:** Conceptualization, Methodology, Investigation, Resources, Writing – review & editing, Funding acquisition, Project administration, Writing – review & editing. **Juan Reyes Larico:** Conceptualization, Methodology, Investigation, Resources, Writing – review & editing, Funding acquisition, Project administration. **Jimena Salcedo Peña:** Methodology, Investigation, Resources. **Huan Fang:** Methodology, Software, Validation. **Kento Magara Gomez:** Writing – review & editing, Investigation. **Jianghanyang Li:** Methodology, Investigation, Writing – review & editing.

Declaration of competing interest

The authors declare that they have no known competing financial interests or personal relationships that could have appeared to influence the work reported in this paper.

Acknowledgment

Funding for this work provided by the Arequipa Nexus Institute for Food, Energy, Water, and the Environment through the Universidad Nacional de San Agustin (UNSA), Arequipa Peru. A cooperation between UNSA and Purdue University, USA. The authors gratefully acknowledge the NOAA Air Resources Laboratory (ARL) for the provision of the HYSPLIT transport and dispersion model and/or READY website (https://www.ready.noaa.gov) used in this publication.

Appendix A. Supplementary data

Supplementary data to this article can be found online at https://doi.org/10.1016/j.atmosenv.2021.118482.

References

Alexander, B., Savarino, J., Barkov, N.I., Delmas, R.J., Thiemens, M.H., 2002. Climate driven changes in the oxidation pathways of atmospheric sulfur. Geophys. Res. Lett. 29 (14) https://doi.org/10.1029/2002GL014879, 30–31–30–4.

Alexander, B., Hastings, M.G., Allman, D.J., Dachs, J., Thornton, J.A., Kunasek, S.A., 2009. Quantifying atmospheric nitrate formation pathways based on a global model of the oxygen isotopic composition (Delta17O) of atmospheric nitrate. Atmos. Chem. Phys. 9 (14), 5043–5056. https://doi.org/10.5194/acp-9-5043-2009.

Alván, A., Jacay, J., Caracciolo, L., Sánchez, E., Trinidad, I., 2018. Sedimentary facies analysis of the Mesozoic clastic rocks in Southern Peru (Tacna, 18°S)_ towards a paleoenvironmental Redefinition and stratigraphic Reorganization. J. S. Am. Earth Sci. 84, 399–421. https://doi.org/10.1016/j.jsames.2018.04.014.

Amrani, A., Said-Ahmad, W., Shaked, Y., Kiene, R.P., 2013. Sulfur isotope homogeneity of oceanic DMSP and DMS. Nat. Acad Sci. 110 (46), 18413–18418. https://doi.org/10.1073/pnas.1312956110/-/DCSupplemental/sapp.pdf.

Andreae, M.O., Ferek, R.J., Bermond, F., Byrd, K.P., Engstrom, R.T., Hardin, S., et al., 1985. Dimethyl sulfide in the marine atmosphere. J. Geophys. Res.: Atmosphere 90 (D7), 12891–12900. https://doi.org/10.1029/JD090iD07p12891.

Arequipa, G.R., Arequipa Gerencia Regional de Salud, 2020. Archivo de datos por el Gerencia Regional de Salud Arequipa 2020. Gerencia Regional De Salud.

Arimoto, R., Kim, Y.J., Kim, Y.P., Quinn, P.K., Bates, T.S., Anderson, T.L., et al., 2006. Characterization of asian dust during ACE-asia. Global Planet. Change 52 (1–4), 23–56. https://doi.org/10.1016/j.gloplacha.2006.02.013.

Baker, A.R., Thomas, M., Bange, H.W., Plasencia Sánchez, E., 2016. Soluble trace metals in aerosols over the tropical south-east Pacific offshore of Peru. Biogeosciences 13 (3), 817–825. https://doi.org/10.5194/bg-13-817-2016.

Bandy, A.R., Thornton, C., Blomquist, B.W., Chen, S., Wade, T.P., Ianni, J.C., et al., 1996. Chemistry of dimethyl sulfide in the equatorial Pacific atmosphere. Geophys. Res. Lett. 23 (7), 741–744.

Bao, H., Thiemens, M.H., 2000. Generation of O2 from BaSO4 using a CO2-laser fluorination system for simultaneous analysis of $\delta^{18}O$ and $\delta^{17}O$. Anal. Chem. 72 (17), 4029–4032. https://doi.org/10.1021/ac000086e.

Bari, A., Ferraro, V., Wilson, L.R., Luttinger, D., Husain, L., 2003. Measurements of gaseous HONO, HNO3, SO2, HCl, NH3, particulate sulfate and PM2.5 in New York, NY. Atmos. Environ. 37 (20), 2825–2835. https://doi.org/10.1016/S1352-2310(03)00199-7.

Berger, I.A., Cooke, R.U., 1997. The origin and distribution of salts on alluvial fans in the Atacama Desert, northern Chile. Earth Surf. Process. Landforms 22 (6), 581–600. https://doi.org/10.1002/(SICI)1096-9837(199706)22:6<581::AID-ESP714>3.0.CO;2-4.

Boon, R., Alexaki, A., Becerra, E.H., 2001. The Ilo Clean Air Project: a local response to industrial pollution control in Peru. Environ. Urbanization 13 (2), 215–232.

Boschetti, T., Cortecci, G., Barbieri, M., Mussi, M., 2007. New and past geochemical data on fresh to brine waters of the Salar de Atacama and Andean Altiplano, northern Chile. Geofluids 7 (1), 33–50. https://doi.org/10.1111/j.1468-8123.2006.00159.x.

Brandt, C., Fabian, I., vanEldik, R., 1995. Transition metal-catalyzed oxidation of Sulfur (IV) oxides, Atmospheric-relevant processes and mechanisms. Chem. Rev. 119–190.

Calhoun, J.A., Bates, T.S., 1989. Sulfur isotope ratios: tracers of non-sea salt sulfate in the remote atmosphere. In: Saltzman, E.S., Cooper, W.J. (Eds.), Presented at the ACS Symposium Series, vol. 393, pp. 367–379 (Washington, D.C).

Calhoun, J.A., Bates, T.S., Charlson, R.J., 1991. Sulfur isotope measurements of submicrometer sulfate aerosol particles over the Pacific Ocean. Geophys. Res. Lett. 18 (10), 1877–1880. https://doi.org/10.1029/91GL02304.

Carmody, R.W., Plummer, N., Busenberg, E., Coplen, T.B., 1998. Methods for Collection of Dissolved Sulfate and Sulfide and Analysis of Their Sulfur Isotopic Composition. USGS Open-File Report, pp. 97–234. https://doi.org/10.3133/ofr97234.

Carn, S.A., Krueger, A.J., Krotkov, N.A., Yang, K., Levelt, P.F., 2007a. Sulfur dioxide emissions from Peruvian copper smelters detected by the Ozone Monitoring Instrument. Geophys. Res. Lett. 34 (9) https://doi.org/10.1029/2006GL029020, 215–5.

Carn, S.A., Krueger, A.J., Krotkov, N.A., Yang, K., Levelt, P.F., 2007b. Sulfur dioxide emissions from Peruvian copper smelters detected by the Ozone Monitoring Instrument. Geophys. Res. Lett. 34 (9), 1–5. https://doi.org/10.1029/2006GL029020.

Carn, S.A., Fioletov, V.E., McLinden, C.A., Li, C., Krotkov, N.A., 2017. A decade of global volcanic SO2 emissions measured from space. Sci. Rep. 1–12. https://doi.org/10.1038/srep44095.

Ccoica-López, K., Pasapera-Gonzales, J., Jimenez, J., 2019. Spatio-Temporal variability of the precipitable water vapor over Peru through MODIS and ERA-interim time series. Atmosphere 10 (4). https://doi.org/10.3390/atmos10040192, 192–19.

Cereceda, P., Osses, P., Larrain, H., Farıas, M., Lagos, M., 2002. Advective, orographic and radiation fog in the Tarapacá region, Chile. Atmos. Res. 64 (1–4), 261–271. https://doi.org/10.1016/s0169-8095(02)00097-2.

Chameides, W.L., Stelson, A.W., 1992. Aqueous-phase chemical processes in deliquescent sea-salt aerosols: a mechanism that couples the atmospheric cycles of S and sea salt. J. Geophys. Res.: Atmosphere 97 (D18), 20565–20580. https://doi.org/10.1029/92JD01923.

Chen, Q., Sheng, L., Gao, Y., Miao, Y., Hai, S., Gao, S., Gao, Y., 2019. The effects of the trans-regional transport of PM2.5 on a heavy haze event in the pearl river Delta in january 2015. Atmosphere 10 (5). https://doi.org/10.3390/atmos10050237, 237–19.

Chester, R., Riley, J.P., 1971. Introduction to Marine Chemistry. Academic Press.

Chin, M., Jacob, D., 1996. Anthropogenic and natural contributions to tropospheric sulfate: a global model analysis. J. Geophys. Res. 101 (D13), 18691–18699.

Chin, M., Savoie, D.L., Huebert, B.J., Bandy, A.R., Thornton, D.C., Bates, T.S., et al., 2000. Atmospheric sulfur cycle simulated in the global model GOCART: comparison with field observations and regional budgets. J. Geophys. Res. 105 (D20), 24–689–24–712.

Chou, C.-L., 2012. Sulfur in coals: a review of geochemistry and origins. Int. J. Coal Geol. 100 (C), 1–13. https://doi.org/10.1016/j.coal.2012.05.009.

Christoforou, C.S., Salmon, L.G., Hannigan, M.P., Solomon, P.A., Cass, G.R., 2011. Trends in fine particle concentration and chemical composition in southern California. J. Air Waste Manag. Assoc. 50 (1), 43–53. https://doi.org/10.1080/10473289.2000.10463985.

Cruz, C., Pandis, S., 2000. Deliquescence and hygroscopic growth of mixed Inorganic–Organic atmospheric aerosol. Environ. Sci. Technol. 34, 4313–4319. https://doi.org/10.1021/es9907109.

Daum, P.H., Sunaid Al, A., Busness, K.M., Hales, J.M., Mazurek, M., 1993. Studies of the Kuwait oil fire plume during midsummer 1991. J. Geophys. Res.: Atmosphere 98 (D9), 16809–16827. https://doi.org/10.1029/93JD01204.

de Bruyn, W.J., Harvey, M., Cainey, J.M., Saltzman, E.S., 2002. DMS and SO2 at baring head, New Zealand: implications for the yield of SO2 from DMS. J. Atmos. Chem. 41 (2), 189–209. https://doi.org/10.1023/A:1014252106572.

del Río, C., Garcia, J.-L., Osses, P., Zanetta, N., Lambert, F., Rivera, D., et al., 2018. ENSO influence on coastal fog-water yield in the Atacama Desert, Chile. Aerosol. Air Qual. Res. 18 (1), 127–144. https://doi.org/10.4209/aaqr.2017.01.0022.

Dentener, F.J., Crutzen, P.J., 1993. Reaction of N2O5 on tropospheric aerosols: impact on the global distributions of NO x, O3, and OH. J. Geophys. Res.: Atmosphere 98 (D4), 7149–7163. https://doi.org/10.1029/92JD02979.

Deshmukh, D.K., Deb, M.K., Tsai, Y.I., Mkoma, S.L., 2011. Water soluble ions in PM2. 5 and PM1 aerosols in Durg city, Chhattisgarh, India. Aerosol. Air Qual. Res. 11, 696–708. https://doi.org/10.4209/aaqr.2010.04.0025.

DIGESA, 2005. Protocolo de monitoreo de la calidad δ aire y gestión de los datos, pp. 1–71. Lima, Peru.
Drewnick, F., Schwab, J.J., Hogrefe, O., Peters, S., Husain, L., Diamond, D., et al., 2003. Intercomparison and evaluation of four semi-continuous PM2.5 sulfate instruments. Atmos. Environ. 37 (24), 3335–3350. https://doi.org/10.1016/S1352-2310(03)00351-0.
Echavarria, L., Nelson, E., Humphrey, J., Escobedo, J., Iriondo, A., 2006. Geologic evolution of the Caylloma epithermal vein district, southern Peru. Econ. Geol. 101 (4), 843–863. https://doi.org/10.2113/gsecongeo.101.4.843.
Eriksson, E., 1960. The yearly circulation of chloride and sulfur in nature; meteorological, geochemical and pedological implications. Part II. Tellus 12 (1), 64–109. https://doi.org/10.3402/tellusa.v12i1.9341.
Feingold, G., Kreidenweis, S.M., Zhang, Y., 1998. Stratocumulus processing of gases and cloud condensation nuclei: 1. Trajectory ensemble model. J. Geophys. Res. 103 (D16), 19–527–19–542.
Félix, O., Csavina, J., Field, J., Rine, K.P., Sáez, A.E., Betterton, E.A., 2015. Use of lead isotopes to identify sources of metal and metalloid contaminants in atmospheric aerosol from mining operations. Chemosphere 122 (C), 219–226. https://doi.org/10.1016/j.chemosphere.2014.11.057.
Forrest, J., Newman, L., 1973. Sampling and analysis of atmospheric sulfur compounds for isotope ratio studies. Atmos. Environ. 7 (5), 561–573.
Francis, T., Sarin, M.M., Rengarajan, R., 2016. Atmospheric SO2 oxidation efficiency over a semi-arid region: seasonal patterns from observations and GEOS-Chem model. Atmos. Environ. 125 (Part B), 383–395. https://doi.org/10.1016/j.atmosenv.2015.09.021.
Gaita, S.M., Boman, J., Gatari, M.J., Pettersson, J.B.C., Janhäll, S., 2014. Source apportionment and seasonal variation of PM 2.5in a Sub-Saharan African city: nairobi, Kenya. Atmos. Chem. Phys. 14 (18), 9977–9991. https://doi.org/10.5194/acp-14-9977-2014.
Galle, B., Johansson, M., Rivera, C., Zhang, Y., Kihlman, M., Kern, C., et al., 2010. Network for Observation of Volcanic and Atmospheric Change (NOVAC)—a global network for volcanic gas monitoring: Network layout and instrument description. J. Geophys. Res. 115 (D5) https://doi.org/10.1029/2009JD011823, 151–19.
Gankanda, A., Coddens, E.M., Zhang, Y., Cwiertny, D.M., Grassian, V.H., 2016. Sulfate formation catalyzed by coal fly ash, mineral dust and iron(iii) oxide: variable influence of temperature and light. Environ. Sci.: Proces. Impacts 18 (12), 1484–1491. https://doi.org/10.1039/C6EM00430J.
Gao, Y.R.A., Duce, R.A., Chen, L.Q., Zhou, M.Y., Gu, D.Y., 1996. Atmospheric non-sea-salt sulfate, nitrate and methanesulfonate over the China Sea. J. Geophys. Res. 101 (D7), 12601–12611.
Garreaud, R.D., Muñoz, R., 2004. The diurnal cycle in circulation and cloudiness over the subtropical southeast Pacific: a modeling study. J. Clim. 17 (8), 1699–1710. https://doi.org/10.2307/26251747.
Graf, H., Feichter, B., Langmann, B., 1997. Volcanic sulfur emissions: estimates of source strength and its contribution to the global sulfate distribution. J. Geophys. Res. 102 (D9), 10727–10738.
Grassineau, N.V., Mattey, P., Lowry, D., 2001. Sulfur isotope analysis of sulfide and sulfate minerals by continuous flow-isotope ratio mass spectrometry. Anal. Chem. 73, 220–225. https://doi.org/10.1021/ac000550f.
Grey, D.C., Jensen, M.L., 1972. Bacteriogenic sulfur in air pollution. Science 177 (4054), 1099–1100.
Guo, Z., Li, Z., Farquhar, J., Kaufman, A.J., Wu, N., Li, C., et al., 2010. Identification of sources and formation processes of atmospheric sulfate by sulfur isotope and scanning electron microscope measurements. J. Geophys. Res. 115 (D14) https://doi.org/10.1029/2009JD012893, 88–13.
Han, Xianglu, Aguilar-Villalobos, M., Allen, J., Carlton, C.S., Robinson, R., Bayer, C., Naeher, L.P., 2005. Traffic-related occupational exposures to PM 2.5, CO, and VOCs in trujillo, Peru. Int. J. Occup. Environ. Health 11 (3), 276–288. https://doi.org/10.1179/107735205800246073.
Han, Xiaokun, Guo, Q., Liu, C., Fu, P., Strauss, H., Yang, J., et al., 2016. Using stable isotopes to trace sources and formation processes of sulfate aerosols from Beijing, China. Sci. Rep. 6, 1–14. https://doi.org/10.1038/srep29958, 29958.
Harris, E., Sinha, B., Hoppe, P., Foley, S., Borrmann, S., 2012. Fractionation of sulfur isotopes during heterogeneous oxidation of SO 2on sea salt aerosol: a new tool to investigate non-sea salt sulfate production in the marine boundary layer. Atmos. Chem. Phys. 12 (10), 4619–4631. https://doi.org/10.5194/acp-12-4619-2012.
Harris, E., Sinha, B., Hoppe, P., Ono, S., 2013. High-precision measurements of 33S and 34S fractionation during SO 2Oxidation reveal causes of seasonality in SO 2and sulfate isotopic composition. Environ. Sci. Technol. 47 (21), 12174–12183. https://doi.org/10.1021/es402824c.
He, P., Alexander, B., Geng, L., Chi, X., Fan, S., Zhan, H., et al., 2018. Isotopic constraints on heterogeneous sulfate production in Beijing haze. Atmos. Chem. Phys. 18 (8), 5515–5528. https://doi.org/10.5194/acp-18-5515-2018.
Hedley, A.J., Wong, C.-M., Thach, T.Q., Ma, S., Lam, T.-H., Anderson, H.R., 2002. Cardiorespiratory and all-cause mortality after restrictions on sulphur content of fuel in Hong Kong: an intervention study. Lancet 360 (9346), 1646–1652. https://doi.org/10.1016/S0140-6736(02)11612-6.
Henmi, T., Reiter, E.R., 1978. Regional residence time of sulfur dioxide over the eastern United States. Atmos. Environ. 12 (6–7), 1489–1495.
Hill, D., 2017, May 1. Peru's Plans to Cut Air Quality Rules Would Smooth Sale of Top Polluter. The Guardian, pp. 1–7.
Hong, Y., Zhang, H., Zhu, Y., 1993. Sulfur isotopic characteristics of coal in China and sulfur isotopic fractionation during coal-burning process. Chin. J. Geochem. 12 (1), 51–59. https://doi.org/10.1007/BF02869045.
Hsieh, L.-Y., Chen, C.-L., Wan, M.-W., Tsai, C.-H., Tsai, Y.I., 2008. Speciation and temporal characterization of dicarboxylic acids in PM2.5 during a PM episode and a period of non-episodic pollution. Atmos. Environ. 42 (28), 6836–6850. https://doi.org/10.1016/j.atmosenv.2008.05.021.
Hsu, S.-C., Liu, S.C., Kao, S.-J., Jeng, W.-L., Huang, Y.-T., Tseng, C.-M., et al., 2007. Water-soluble species in the marine aerosol from the northern South China Sea: high chloride depletion related to air pollution. J. Geophys. Res. 112 (D19) https://doi.org/10.1029/2007JD008844, 2011–11.
Huamán De La Cruz, A., Bendezu Roca, Y., Suarez-Salas, L., Pomalaya, J., Alvarez Tolentino, D., Gioda, A., 2019. Chemical characterization of PM2.5 at rural and urban sites around the metropolitan area of huancayo (central Andes of Peru). Atmosphere 10 (21), 1–17. https://doi.org/10.3390/atmos10010021.
Huneeus, N., Gallardo, L., Rutllant, J.A., 2006. Offshore transport episodes of anthropogenic sulfur in northern Chile: potential impact on the stratocumulus cloud deck. Geophys. Res. Lett. 33 (19), 25251–25255. https://doi.org/10.1029/2006GL026921.
INGEMMET, 2018. Información Sobre Monitoreo Volcánico 2018 Reporte Semanal. http://ovi.ingemmet.gob.pe. (Accessed 13 November 2020).
INGEMMET, 2020. Información Sobre Monitoreo Volcánico 2020 Reporte Subanal. http://ovi.inemmet.gob.pe. (Accessed 13 November 2020).
Kanaya, Y., Cao, R., Akimoto, H., Fukuda, M., Komazaki, Y., Yokouchi, Y., et al., 2007. Urban photochemistry in central Tokyo: 1. Observed and modeled OH and HO 2radical concentrations during the winter and summer of 2004. J. Geophys. Res. 112 (D21) https://doi.org/10.1029/2007JD008670, 8196–20.
Kerminen, V.M., Hillamo, R., Teinilä, K., Atmospheric, T.P., 2001. Ion balances of size-resolved tropospheric aerosol samples: implications for the acidity and atmospheric processing of aerosols. Atmos. Environ. 35 (31), 5255–5265. https://doi.org/10.1016/S1352-2310(01)00345-4, 2001.
Khokhar, M.F., Platt, U., Wagner, T., 2008. Temporal trends of anthropogenic SO2 emitted by non-ferrous metal smelters in Peru and Russia estimated from Satellite observations. Atmos. Chem. Phys. Discuss. 8, 17393–17422.
Kim, B.M., Teffera, S., Zeldin, M.D., 2011. Characterization of PM 25and PM 10in the south coast air basin of southern California: Part 1—spatial variations. J. Air Waste Manag. Assoc. 50 (12), 2034–2044. https://doi.org/10.1080/10473289.2000.10464242.
Kistler, R.B., Helvaci, C., 1994. Boron and borates. Ind. Miner. Rocks 6, 171–186.
Klein, S.A., Hartman, D.L., 1993. The seasonal cycle of low stratiform clouds. J. Clim. 6 (8), 1587–1606.
Koike, M., Kondo, Y., Kita, K., Takegawa, N., Masui, Y., Miyazaki, Y., et al., 2003. Export of anthropogenic reactive nitrogen and sulfur compounds from the East Asia region in spring. J. Geophys. Res. 108 (D20) https://doi.org/10.1029/2002JD003284, 23,097–19.
Kondo, Y., Miyazaki, Y., Takegawa, N., Miyakawa, T., Weber, R.J., Jimenez, J.L., et al., 2007. Oxygenated and water-soluble organic aerosols in Tokyo. J. Geophys. Res. 112 (D1) https://doi.org/10.1029/2006JD007056, 5745–11.
Krouse, H.R., 1977. Sulphur isotope abundance elucidate uptake of atmospheric sulphur emissions by vegetation. Nature 265 (5589), 45–46.
Krouse, H.R., Grinenko, V.A. (Eds.), 1991. Scope 43: Stable Isotopes: Natural and Anthropogenic Sulphur in the Environment. John Wiley & Sons.
Lana, A., Bell, T.G., Simó, R., Vallina, S.M., Ballabrera-Poy, J., Kettle, A.J., et al., 2011. An updated climatology of surface dimethlysulfide concentrations and emission fluxes in the global ocean. Global Biogeochem. Cycles 25 (GB1004), 1–17. https://doi.org/10.1029/2010GB003850.
Larrea Valdivia, A.E., Reyes Larico, J.A., Salcedo Peña, J., Wannaz, E.D., 2019. Health risk assessment of polycyclic aromatic hydrocarbons (PAHs) adsorbed in PM2.5 and PM10 in a region of Arequipa, Peru. Environ. Sci. Pollut. Res. 27, 3065–3075. https://doi.org/10.1007/s11356-019-07185-5.
Li, J., Michalski, G., Davy, P., Harvey, M., Katzman, T., Wilkins, B., 2018. Investigating source contributions of size-aggregated aerosols collected in southern ocean and baring head, New Zealand using sulfur isotopes. Geophys. Res. Lett. 45 (8), 3717–3727. https://doi.org/10.1002/2018GL077353.
Li, J., Wang, F., Michalski, G., Wilkins, B., 2019. Atmospheric deposition across the Atacama Desert, Chile_ Compositions, source distributions, and interannual comparisons. Chem. Geol. 525, 435–446. https://doi.org/10.1016/j.chemgeo.2019.07.037.
Li, J., Zhang, Y.-L., Cao, F., Zhang, W., Fan, M., Lee, X., Michalski, G., 2020. Stable sulfur isotopes revealed a major role of transition-metal ion-catalyzed SO2 oxidation in haze episodes. Environ. Sci. Technol. 1–9. https://doi.org/10.1021/acs.est.9b07150.
Liu, X., Penner, J.E., Herzog, M., 2005. Global modeling of aerosol dynamics: model description, evaluation, and interactions between sulfate and nonsulfate aerosols. J. Geophys. Res. 110 (D18) https://doi.org/10.1029/2004JD005674, 3661–37.
Marini, L., Moretti, R., Accornero, M., 2011. Sulfur isotopes in magmatic-hydrothermal systems, melts, and magmas. Rev. Mineral. Geochem. 73 (1), 423–492. https://doi.org/10.2138/rmg.2011.73.14.
Mariotti, A., Germon, J.C., Hubert, P., Kaiser, P., Letolle, R., Tardieux, A., Tardieux, P., 1981. Experimental determination of nitrogen kinetic isotope fractionation: some principles; illustration for the denitrification and nitrification processes. Plant Soil 62 (3), 413–430. https://doi.org/10.1007/BF02374138.
Marshall, L., Schmidt, A., Toohey, M., Carslaw, K.S., Mann, G.W., Sigl, M., et al., 2018. Multi-model comparison of the volcanic sulfate deposition from the 1815 eruption of Mt. Tambora. Atmos. Chem. Phys. 18 (3), 2307–2328. https://doi.org/10.5194/acp-18-2307-2018.
Mayer, B., Alpay, S., Gould, W.D., Lortie, L., Rosa, F., 2007. The onset of anthropogenic activity recorded in lake sediments in the vicinity of the Horne smelter in Quebec, Canada: sulfur isotope evidence. Appl. Geochem. 22 (2), 397–414. https://doi.org/10.1016/j.apgeochem.2006.10.001.
McKeen, S., Chung, S.H., Wilczak, J., Grell, G., Djalalova, I., Peckham, S., et al., 2007. Evaluation of several PM 2.5 forecast models using data collected during the

ICARTT/NEAQS 2004 field study. J. Geophys. Res.: Atmosphere 112 (D10). https://doi.org/10.1029/2006JD007608, 2981–20.
Meixner, F.X., Eugster, W., 1999. Effects of landscape pattern and topography on emissions and transport. In: Tenhunen, J.D., Kabat, P. (Eds.), Integrating Hydrology, Ecosystem Dynamics, and Biogeochemistry in Complex Landscapes.
MINAM. Aprueban Estándares de Calidad Ambiental (ECA) para Aire y establecen Disposiciones Complementarias (558 ed.) (pp. 1–4). El Peruano.
Mining data online, 2020. Mining Data Solutions Ilo Smelter and Refinery. Retrieved October 12, 2020, from. https://miningdataonline.com/property/1481/Ilo-Plant.aspx.
Moussallam, Y., Tamburello, G., Peters, N., Apaza, F., Schipper, C.I., Curtis, A., et al., 2017. Volcanic gas emissions and degassing dynamics at Ubinas and Sabancaya volcanoes; implications for the volatile budget of the central volcanic zone. J. Volcanol. Geoth. Res. 343 (C), 181–191. https://doi.org/10.1016/j.jvolgeores.2017.06.027.
Norman, A.L., Barrie, A., Toom-Sauntry, D., Sirois, A., Krouse, H.R., Li, S.M., Sharma, S., 1999. Sources of aerosol sulphate at Alert: apportionment using stable isotopes. J. Geophys. Res. 104 (D9), 11619–11631.
Norman, A.-L., Anlauf, K., Hayden, K., Thompson, B., Brook, J.R., Li, S.-M., Bottenheim, J., 2006. Aerosol sulphate and its oxidation on the Pacific NW coast: S and O isotopes in PM2.5. Atmos. Environ. 40 (15), 2676–2689. https://doi.org/10.1016/j.atmosenv.2005.09.085.
Oduro, H., Van Alstyne, K.L., Farquhar, J., 2012. Sulfur isotope variability of oceanic DMSP generation and its contributions to marine biogenic sulfur emissions. Nat. Acad Sci. 109 (23), 9012–9016. https://doi.org/10.1073/pnas.1117691109/-/DCSupplemental.
Osornio-Vargas, A.R., Serrano, J., Rojas-Bracho, L., Miranda, J., García-Cuellar, C., Reyna, M.A., et al., 2011. In vitro biological effects of airborne PM2.5 and PM10 from a semi-desert city on the Mexico–US border. Chemosphere 83 (4), 618–626. https://doi.org/10.1016/j.chemosphere.2010.11.073.
Parnell, A.C., Phillips, D.L., Bearhop, S., Semmens, B.X., Ward, E.J., Moore, J.W., et al., 2013. Bayesian stable isotope mixing models. Environmetrics 10 (1–2), 387–399. https://doi.org/10.1002/env.2221.
Pattantyus, A.K., Businger, S., Howell, S.G., 2018. Review of sulfur dioxide to sulfate aerosol chemistry at Kīlauea Volcano. Hawai'i. Atmos. Environ. 185, 262–271. https://doi.org/10.1016/j.atmosenv.2018.04.055.
Pearce, J.L., Aguilar-Villalobos, M., Rathbun, S.L., Naeher, L.P., 2009. Residential exposures to PM 2.5and CO in cusco, A high-altitude city in the Peruvian Andes: a pilot study. Arch. Environ. Occup. Health 64 (4), 278–282. https://doi.org/10.1080/19338240903338205.
Pope III, C.A., Dockery, D.W., 2012. Health effects of fine particulate air pollution: lines that connect. J. Air Waste Manag. Assoc. 56 (6), 709–742. https://doi.org/10.1080/10473289.2006.10464485.
Pueyo, J.J., Chong, G., Jensen, A., 2001. Neogene evaporites in desert volcanic environments: Atacama Desert, northern Chile. Sedimentology 48 (6), 1411–1431. https://doi.org/10.1046/j.1365-3091.2001.00428.x.
Quinn, P.K., Bates, T.S., 2005. Regional aerosol properties: comparisons of boundary layer measurements from ACE 1, ACE 2, Aerosols99, INDOEX, ACE Asia, TARFOX, and NEAQS. J. Geophys. Res.: Atmosphere 110 (D14), 1–24. https://doi.org/10.1029/2004JD004755.
Quinn, P.K., Bates, T.S., Coffman, D.J., Miller, T.L., Johnson, J.E., Covert, D.S., et al., 2000. A comparison of aerosol chemical and optical properties from the 1st and 2nd Aerosol Characterization Experiments. Tellus B 52 (2), 239–257. https://doi.org/10.3402/tellusb.v52i2.16103.
Rankin, A.J., 2012, August 22. Predicted Ash Hazards from Potential Eruptions at Nevado Sabancaya, Peru: HYSPLIT and Remote Sensing.
Rayleigh, L., 1896. L. Theoretical considerations respecting the separation of gases by diffusion and similar processes. The London, Edinburgh, and Dublin. Philosop. Magaz. J. Sci. 42 (259), 493–498. https://doi.org/10.1080/14786449608620944.
Reath, K., Pritchard, M.E., Moruzzi, S., Alcott, A., Coppola, D., Pieri, D., 2019. The AVTOD (ASTER volcanic thermal output database) Latin America archive. J. Volcanol. Geoth. Res. 376, 62–74. https://doi.org/10.1016/j.jvolgeores.2019.03.019.
Rech, J.A., Quade, J., Hart, W.S., 2003. Isotopic evidence for the source of Ca and S in soil gypsum, anhydrite and calcite in the Atacama Desert, Chile. Geochem. Cosmochim. Acta 67 (4), 575–586. https://doi.org/10.1016/S0016-7037(02)01175-4.
Rempillo, O., Seguin, A.M., Norman, A.-L., Scarratt, M., Michaud, S., Chang, R., et al., 2011. Dimethyl sulfide air-sea fluxes and biogenic sulfur as a source of new aerosols in the Arctic fall. J. Geophys. Res. 116 (C3) https://doi.org/10.1029/2011JD016336, 366–15.
Ren, X., Brune, W.H., Mao, J., Mitchell, M.J., Lesher, R.L., Simpas, J.B., et al., 2006. Behavior of OH and HO2 in the winter atmosphere in New York City. Atmos. Environ. 40, 252–263. https://doi.org/10.1016/j.atmosenv.2005.11.073.
Rodríguez, S., Alastuey, A., Alonso-Pérez, S., Querol, X., Cuevas, E., Abreu-Afonso, J., et al., 2011. Transport of desert dust mixed with North African industrial pollutants in the subtropical Saharan Air Layer. Atmos. Chem. Phys. 11 (13), 6663–6685. https://doi.org/10.5194/acp-11-6663-2011.
Rutllant, J.A., Garreaud, R., 2004. Episodes of strong flow down the western slope of the subtropical Andes. J. Clim. 132 (2), 611–622. https://doi.org/10.1175/1520-0493(2004)132<0611:EOSFDT>2.0.CO;2.
Saltzman, E.S., Savoie, D.L., Prospero, J.M., Zika, R.G., Mosher, B., 1986. Elevated atmospheric sulfur levels off the Peruvian coast. J. Geophys. Res.: Atmosphere 91 (D7), 7913–7918.
Sandor, J.A., Furbee, L., 1996. Indigenous knowledge and classification of soils in the Andes of southern Peru. Soil Sci. Soc. Am. J. 60 (5), 1502–1512. https://doi.org/10.2136/sssaj1996.03615995006000050031x.
Schmitt, A.K., Kasemann, S., Meixner, A., Geology, D.R.C., 2002. Boron in central Andean ignimbrites: implications for crustal boron cycles in an active continental margin. Atmos. Environ. 183 (1–4), 333–347. https://doi.org/10.1016/S0009-2541(01)00382-5, 2002.
Seinfeld, John H, Pandis, Spyros N., 2016. Chapter 6. Chemistry of the Troposphere. Atmospheric chemistry and physics: from air pollution to climate change. John Wiley & Sons, pp. 175–259.
Shahid, Imran, Kistler, Magdalena, Mukhtar, Azam, Ghauri, Badar M., Cruz, Carlos Ramirez-Santa, Bauer, Heidi, Puxbaum, Hans, 2016. Chemical characterization and mass closure of PM10 and PM2.5 at an urban site in Karachi – Pakistan. Atmos. Environ. 128, 114–123.
Shaltout, A.A., Boman, J., Dhaif-allah, R., Shehadeh, Z.F., 2013. Elemental composition of $PM_{2.5}$ particles sampled in industrial and residential areas of Taif, Saudi Arabia. Aerosol Air Qual. Res. 13 (4), 1356–1364.
Singer, A., Shamay, Y., Fried, M., 1993. Acid rain on Mt carmel, Israel. Atmos. Environ. 27A (15), 2287–2293.
Smith, S.J., Pitcher, H., Wigley, T.M.L., 2001. Global and regional anthropogenic sulfur dioxide emissions. Global Planet. Change 29 (1–2), 99–119. https://doi.org/10.1016/S0921-8181(00)00057-6.
Snider, G., Weagle, C.L., Murdymootoo, K.K., Ring, A., Ritchie, Y., Stone, E., et al., 2016. Variation in global chemical composition of PM 2.5: emerging results from SPARTAN. Atmos. Chem. Phys. 16 (15), 9629–9653. https://doi.org/10.5194/acp-16-9629-2016.
Stein, A.F., Draxler, R.R., Rolph, G.D., Stunder, B.J.B., Cohen, M.D., Ngan, F., 2015. NOAA's HYSPLIT atmospheric transport and dispersion modeling system. Bull. Am. Meteorol. Soc. 96 (12), 2059–2077. https://doi.org/10.1175/BAMS-D-14-00110.1.
Stockwell, W.R., Kirchner, F., Kuhn, M., Seefeld, S., 1997. A new mechanism for regional atmospheric chemistry modeling. J. Geophys. Res.: Atmosphere 102 (D22), 25847–25879. https://doi.org/10.1029/97JD00849.
Sträter, E., Westbeld, A., Klemm, O., 2010. Pollution in coastal fog at alto patache, northern Chile. Environ. Sci. Pollut. Res. Int. 17 (9), 1563–1573. https://doi.org/10.1007/s11356-010-0343-x.
Tanaka, N., Rye, D.M., Xiao, Y., Lasaga, A.C., 1994. Use of stable sulfur isotope systematics for evaluating oxidation reaction pathways and in-cloud-scavenging of sulfur dioxide in the atmosphere. Geophys. Res. Lett. 21 (14), 1519–1522. https://doi.org/10.1029/94GL00893.
US EPA, 1995. Background Report AP-42 12.3 Primary Copper Smelting, pp. 1–44 (Research Triangle Park, NC).
Valdivia-Silva, J.E., Navarro-González, R., McKay, C., 2009. Thermally evolved gas analysis (TEGA) of hyperarid soils doped with microorganisms from the Atacama Desert in southern Peru: implications for the Phoenix mission. Adv. Space Res. 44 (2), 254–266. https://doi.org/10.1016/j.asr.2009.02.008.
Vasconcellos, P.C., Souza, D.Z., Ávila, S.G., Araújo, M.P., Naoto, E., Nascimento, K.H., et al., 2011. Comparative study of the atmospheric chemical composition of three South American cities. Atmos. Environ. 45 (32), 5770–5777. https://doi.org/10.1016/j.atmosenv.2011.07.018.
Voigt, C., Klipsch, S., Herwartz, D., Chong, G., Staubwasser, M., 2020. The spatial distribution of soluble salts in the surface soil of the Atacama Desert and their relationship to hyperaridity. Global Planet. Change 184, 103077. https://doi.org/10.1016/j.gloplacha.2019.103077.
Wallace, J., Corr, D., Kanaroglou, P., 2010. Topographic and spatial impacts of temperature inversions on air quality using mobile air pollution surveys. Sci. Total Environ. 408 (21), 5086–5096. https://doi.org/10.1016/j.scitotenv.2010.06.020.
Wang, T., Guo, H., Blake, D.R., Kwok, Y.H., Simpson, I.J., Li, Y.S., 2005. Measurements of trace gases in the inflow of South China sea background air and outflow of regional pollution at tai O, southern China. J. Atmos. Chem. 52 (3), 295–317. https://doi.org/10.1007/s10874-005-2219-x.
Wang, Y., Zhuang, G., Zhang, X., Huang, K., Xu, C., Tang, A., et al., 2006. The ion chemistry, seasonal cycle, and sources of PM2.5 and TSP aerosol in Shanghai. Atmos. Environ. 40 (16), 2935–2952. https://doi.org/10.1016/j.atmosenv.2005.12.051.
Wang, F., Michalski, G., Seo, J.-H., Ge, W., 2014. Geochemical, isotopic, and mineralogical constraints on atmospheric deposition in the hyper-arid Atacama Desert, Chile. Geochem. Cosmochim. Acta 135 (C), 29–48. https://doi.org/10.1016/j.gca.2014.03.017.
Weatheronlineuk, 2019, February 2. Weather online. Retrieved August 12, 2019, from. https://www.weatheronline.co.uk/.
WHO, 2006. WHO Air Quality Guidelines for Particulate Matter, Ozone, Nitrogen Dioxide and Sulfur Dioxide. World Health Organization Publications, Geneva, Switzerland, pp. 1–22.
Wu, F., Zhang, D., Cao, J., Xu, H., An, Z., 2012. Soil-derived sulfate in atmospheric dust particles at Taklimakan desert. Geophys. Res. Lett. 39 (24) https://doi.org/10.1029/2012GL054406, 127–6.
Wu, Y., Xu, Z., Liu, W., Zhao, T., Zhang, X., Jiang, H., et al., 2016. Chemical compositions of precipitation at three non-urban sites of Hebei Province, North China: influence of terrestrial sources on ionic composition. Atmos. Res. 181 (C), 115–123. https://doi.org/10.1016/j.atmosres.2016.06.009.
Xiao, H.-W., Xiao, H.-Y., Long, A.-M., Wang, Y.-L., Liu, C.-Q., 2014. Sources and meteorological factors that control seasonal variation of δ34S values in rainwater. Atmos. Res. 149 (C), 154–165. https://doi.org/10.1016/j.atmosres.2014.06.003.

Yao, X., Chan, C.K., Fang, M., Cadle, S., Chan, T., Mulawa, P., et al., 2002. The water-soluble ionic composition of PM2.5 in Shanghai and Beijing, China. Atmos. Environ. 36 (26), 4223–4234. https://doi.org/10.1016/S1352-2310(02)00342-4.

Zhou, Q., Li, J., Xu, J., Qin, X., Deng, C., Fu, J.S., et al., 2018. First long-term detection of paleo- oceanic signature of dust aerosol at the southern marginal area of the Taklimakan Desert. Sci. Rep. 1–9. https://doi.org/10.1038/s41598-018-25166-5.

Ziemba, L.D., Fischer, E., Griffin, R.J., Talbot, R.W., 2007. Aerosol acidity in rural New England: temporal trends and source region analysis. J. Geophys. Res.: Atmosphere 112 (D10). https://doi.org/10.1029/2006JD007605, 221–13.